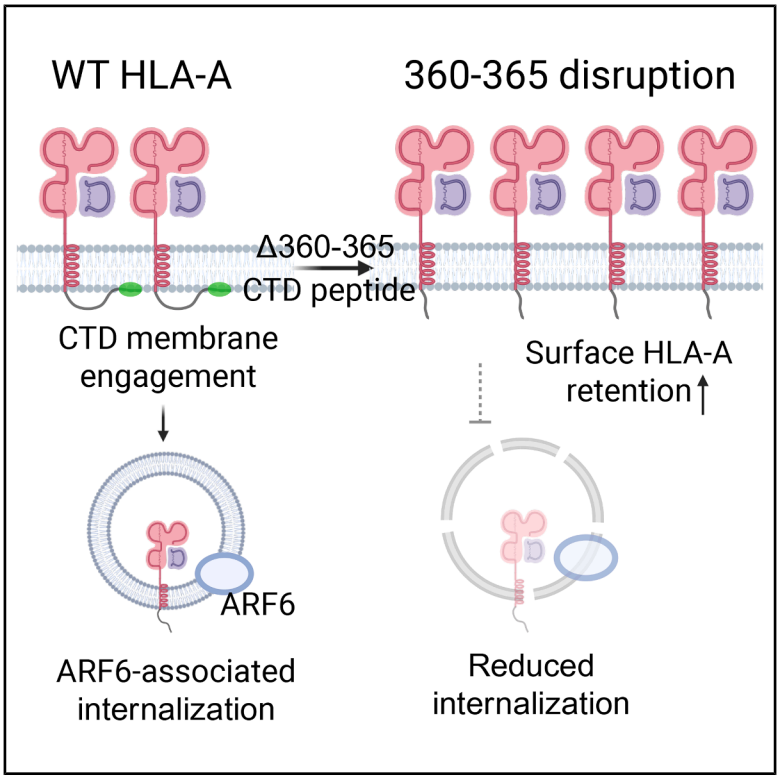
Cell Reports

Article

Membrane engagement by the HLA-A cytoplasmic tail regulates endocytosis and surface retention

Graphical abstract



Authors

Xi Xu, Yuxuan Wang, Yihuang Wu, ..., Zhifeng Chen, James J. Chou, Linlin Zhao

Correspondence

2305635@tongji.edu.cn (Z.C.), james_chou@mail.sioc.ac.cn (J.J.C.), lzhao@tongji.edu.cn (L.Z.)

In brief

Xu et al. identify a membrane responsive segment in the HLA-A cytoplasmic tail that promotes receptor internalization and limits surface retention. Disrupting this region, genetically or with a tail-derived peptide, reduces internalization and preserves surface HLA-I, revealing a receptor intrinsic mechanism that regulates antigen presenting complex availability.

Highlights

- HLA-A*11:01 tail residues 360–365 engage phospholipid membranes
- Cys363 and the transmembrane region shape HLA-A molecular proximity
- The 360–365 region promotes HLA-A internalization and protein turnover
- A tail-derived peptide enhances endogenous HLA-I surface retention

Xu et al., 2026, Cell Reports *45*, 117940
September 22, 2026 © 2026 The Author(s). Published by Elsevier Inc.
https://doi.org/10.1016/j.celrep.2026.117940

CellPress

Cell Reports

CellPress
OPEN ACCESS

Article

Membrane engagement by the HLA-A cytoplasmic tail regulates endocytosis and surface retention

Xi Xu,[1,7] Yuxuan Wang,[1,7] Yihuang Wu,[1] Zhenjia Cai,[1] Jiali Zhu,[1,4] Hui Wu,[1] Maorong Wen,[2] Hongjuan Xue,[3] Jingxin Liu,[4] Zhifeng Chen,[1,*] James J. Chou,[5,6,*] and Linlin Zhao[1,8,*]

[1]Department of Anesthesiology, Putuo People's Hospital, School of Medicine, Tongji University, Shanghai 200060, China
[2]Hangzhou Weizhi Biotechnology Co., Ltd, Hangzhou 310012, China
[3]National Facility for Protein Science in Shanghai, ZhangJiang Lab, Shanghai Advanced Research Institute, Chinese Academy of Sciences, Shanghai 201210, China
[4]Tongji University Cancer Center, Shanghai Tenth People's Hospital, School of Medicine, Tongji University, Shanghai 200072, China
[5]State Key Laboratory of Chemical Biology, Shanghai Institute of Organic Chemistry, Chinese Academy of Sciences, Shanghai 200032, China
[6]Interdisciplinary Research Center on Biology and Chemistry, Shanghai Institute of Organic Chemistry, Chinese Academy of Sciences, Shanghai 201203, China
[7]These authors contributed equally
[8]Lead contact
*Correspondence: 2305635@tongji.edu.cn (Z.C.), james_chou@mail.sioc.ac.cn (J.J.C.), lzhao@tongji.edu.cn (L.Z.)
https://doi.org/10.1016/j.celrep.2026.117940

SUMMARY

Loss of major histocompatibility complex class I (MHC-I) molecules from the tumor cell surface is a common mechanism of immune evasion; yet, the receptor intrinsic events that initiate their endocytic removal remain unclear. Here, using HLA-A*11:01, a human MHC-I heavy chain allotype as a model, we identify a membrane responsive regulatory module within its cytoplasmic tail. The conserved 360–365 segment engages phospholipid membranes and undergoes Cys363-dependent self-association under membrane mimetic conditions, while cooperating with the transmembrane region to shape the molecular proximity of full-length HLA-A. Disruption of this segment weakens association with the trafficking GTPase ARF6, slows receptor internalization, and prolongs HLA-A retention at the cell surface. Consistently, a cell penetrating peptide containing this sequence limits endogenous HLA-A internalization across several tumor cell lines. These findings identify the HLA-A cytoplasmic tail as an active regulator of endocytic trafficking and suggest a strategy for preserving surface HLA-A availability in tumor cells.

INTRODUCTION

Major histocompatibility complex class I (MHC-I) molecules play a pivotal role in tumor immunotherapy by presenting tumor antigenic peptides that are recognized by the T cell receptors (TCRs) of cytotoxic T cells.[1,2] This immune synapse is crucial for the efficacy of TCR-engineered T cell therapies and immune checkpoint blockade therapies. However, clinical observations have revealed frequent loss or downregulation of MHC-I antigens in multiple tumor types, including pancreatic, non-small cell lung, breast, and colorectal cancers.[3–8] Such antigen loss weakens T cell recognition and facilitates tumor immune escape. Understanding how MHC-I surface expression is regulated is therefore essential for improving the efficacy of immunotherapies.

Tumor cells employ diverse mechanisms to reduce MHC-I abundance on the plasma membrane. Genetic mutations or deletions in components of the MHC-I presentation pathway, such as TAP, tapasin, proteasomal subunits, or β_2-microglobulin (β2M), impair proper MHC-I assembly and peptide loading.[3,9] These irreversible alterations are complemented by reversible, non-genetic mechanisms. Epigenetic silencing and transcriptional repression can suppress MHC-I expression,[10–12] while post-translational degradation further reduces its surface availability. In particular, autophagy and the ubiquitin proteasome system have emerged as critical regulators of MHC-I homeostasis. In pancreatic cancer, the autophagy receptor NBR1 selectively targets MHC-I for degradation in autolysosomes, and inhibiting this process restores MHC-I surface expression and enhances $CD8^+$ T cell recognition.[13] Similarly, IRGQ acts as an autophagy receptor engaging GABARAP and LC3B, suppressing MHC-I expression at both transcript and protein levels, whereas IRGQ downregulation promotes antigen presentation.[14] In addition, glucocorticoid receptor overexpression can reduce MHC-I via autophagy in pancreatic cancer.[15] Blocking these degradation pathways synergizes with immunotherapies to improve tumor clearance.[16–18] The ubiquitin proteasome system also contributes to MHC-I turnover: in acute myeloid leukemia, SUSD6 and TMEM127 promote MHC-I ubiquitination and degradation, while TMEM127 disruption stabilizes MHC-I and enhances immune recognition.[19] Compared with genetic defects, targeting these degradation pathways provides reversible and therapeutically tractable opportunities to restore MHC-I surface expression.

This is an open access article under the CC BY license (http://creativecommons.org/licenses/by/4.0/).

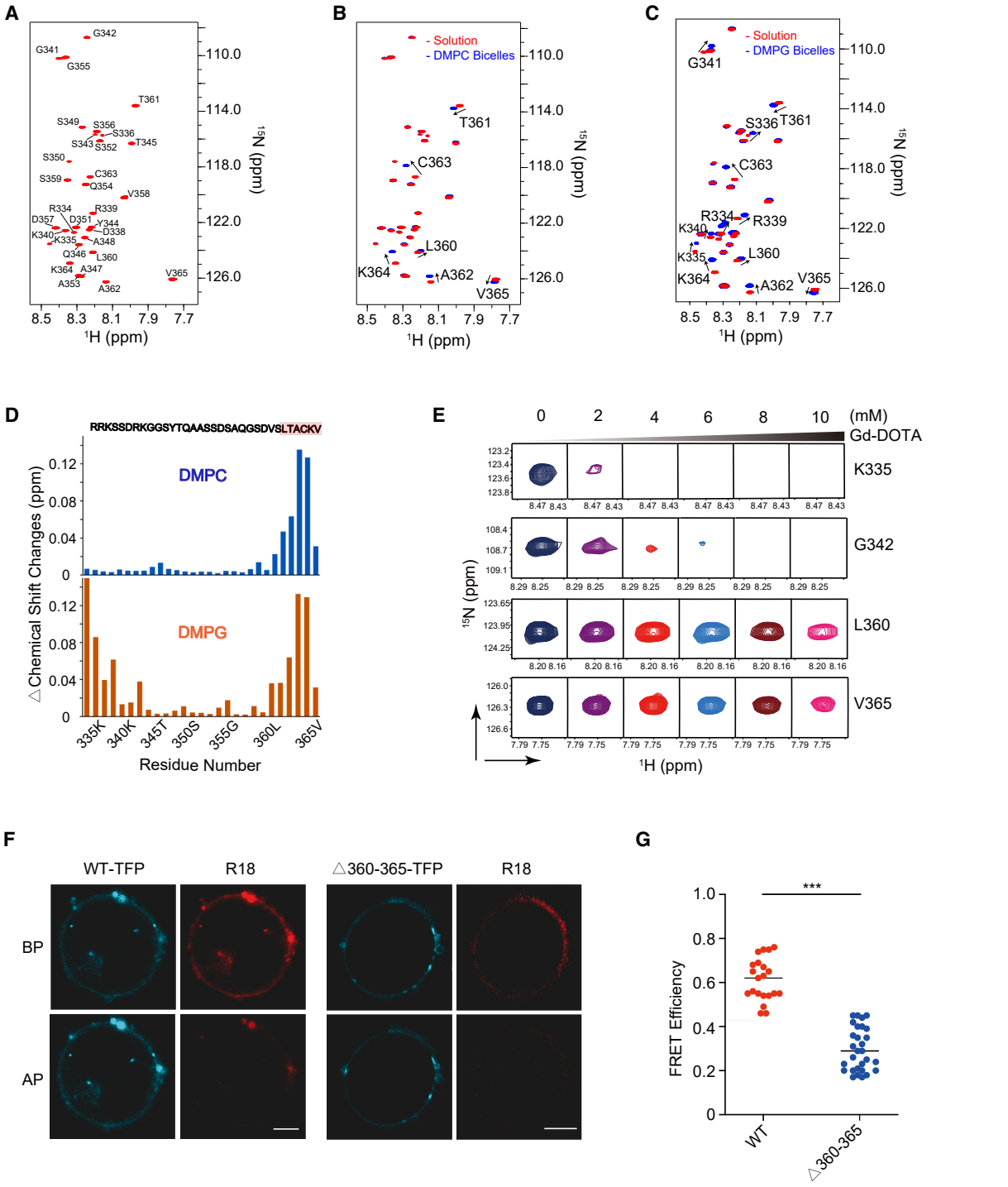


Figure 1. The HLA-A 360–365 motif engages membrane mimetics through charge independent phospholipid interactions

(A) ^{1}H-^{15}N TROSY-HSQC spectrum of the HLA-A-CTD (residues 333–365) in solution, with backbone resonance assignments. Data were acquired at a ^{1}H frequency of 600 MHz using [^{15}N/^{13}C]- labeled protein in 25 mM phosphate, 100 mM NaCl, pH 6.5.

(B and C) Superimposed ^{1}H-^{15}N TROSY-HSQC spectra of HLA-A-CTD in aqueous buffer (red) versus zwitterionic DMPC/DH$_6$PC bicelles (q = 0.8) (B) or anionic DMPG/DH$_6$PC bicelles (q = 0.8) (C). Arrows indicate residues with significant CSPs (ΔCSPs > 0.04 ppm).

(D) Quantification of CSPs induced by DMPC (blue) or DMPG (orange) relative to apo.

(legend continued on next page)

Despite these advances, the receptor intrinsic features that regulate human leukocyte antigen class I (HLA-I) removal from the plasma membrane remain incompletely understood. Degradation of the peptide-MHC complex, whether mediated by autophagy or the proteasome, begins with MHC-I internalization from the plasma membrane, a crucial initiating step that remains poorly understood. Internalization is generally facilitated by adaptor mediated endocytosis, which enables MHC-I entry into the cytoplasmic degradation routes.[20–22] Endocytosis typically proceeds through either clathrin mediated or clathrin independent pathways.[23,24] The former relies on adaptor proteins such as AP2 to recruit clathrin and form coated pits,[25,26] whereas the latter involves small GTPases including ARF family members, caveolae, and flotillin associated mechanisms.[27–29] Among these, the small GTPase ARF6 has been implicated in MHC-I internalization.[30,31] However, how structural features of the HLA-A cytoplasmic tail relate to ARF6-associated surface trafficking remains unclear.

Structurally, MHC-I molecules consist of a heavy chain encoded by HLA genes and a light chain (β2M). Their cytoplasmic tail domain (CTD), encoded by exons 6 and 7, is a short cytoplasmic segment that dictates membrane localization and protein-protein interactions.[32,33] Although CTDs of many transmembrane proteins comprise only short peptide segments, they are critical for maintaining receptor stability and regulating downstream signaling. Immune receptors such as CD3ε and CD28 contain ITAM motifs (YxxL/Ix$_{6-8}$YxxL/I) that associate with negatively charged phospholipids via adjacent basic residue sequences (BRSs), stabilizing the receptor in a resting state.[34–36] T cell activation triggers calcium influx, which disrupts this interaction and initiates signal transduction. Similarly, the intracellular domain of PD-L1 contains a conserved BRS that interacts with the plasma membrane to shield lysine residues from ubiquitination, thereby stabilizing PD-L1 at the cell surface and facilitating immune evasion.[37]

Here, we identify a previously unrecognized lipid binding feature within the intracellular domain of HLA-A. Specifically, we focus on a conserved C-terminal motif (residues 360–365) of HLA-A and examine its capacity to interact with membrane phospholipids. Using biochemical, biophysical, and cell-based approaches, we examined whether this segment engages phospholipid membrane mimetics and how this membrane responsive behavior relates to HLA-A surface trafficking. We further examined whether this region is linked to ARF6-associated trafficking and the regulation of HLA-A surface retention. Through this framework, our study examines how a membrane responsive feature of the HLA-A cytoplasmic tail contributes to surface trafficking and receptor retention.

RESULTS

HLA-A C-terminal domain (360–365) shows non-electrostatic interactions with simulated membrane lipid system

Sequence comparison of the 50 most prevalent alleles at each HLA-A, HLA-B, and HLA-C[38] showed that the C-terminal 360–365 like segment is retained in most, but not all, HLA-A alleles, whereas the corresponding regions of HLA-B and HLA-C display only partial sequence conservation (Figure S1A). We therefore selected the HLA-A*11:01 cytoplasmic tail (HLA-A*11:01-CTD) as the primary model for mechanistic analysis and prepared high-purity samples in neutral phosphate buffer (Figures S1B–S1D). Backbone resonance assignments were completed by solution-state NMR to enable residue-resolved mapping (Figure 1A). To mimic key phospholipid environments, bicelles containing either neutral 1,2-dimyristoyl-*sn*-glycero-3-phosphocholine (DMPC) or acidic DMPG were prepared and used for NMR titrations with HLA-A*11:01-CTD. DMPC induced prominent chemical shift perturbations (CSPs) that were highly localized to residues 360–365, whereas other regions showed minimal changes (Figure 1B). In contrast, DMPG additionally perturbed the membrane proximal BRS, consistent with electrostatic engagement of acidic phospholipids (Figures 1C and 1D). These data identify a discrete C-terminal segment (360–365) that engages phospholipid membranes in a manner separable from the canonical BRS-anionic lipid interaction.

Consistent with a direct membrane engagement model, we next examined whether the DMPC dependent CSPs reflected physical insertion of the 360–365 segment into the membrane mimetic. Paramagnetic relaxation enhancement (PRE) NMR experiments were performed using the water-soluble probe Gd-DOTA in the presence of DMPC bicelles, and residue specific PRE amplitudes were quantified. The 360–365 segment exhibited the lowest PRE$_{amp}$ values along the polypeptide chain, indicating maximal protection from solvent and supporting its insertion into the lipid environment (Figure 1E; Figure S1E).

We then performed fluorescence-resonance energy transfer (FRET) analysis to further investigate the membrane binding behavior of the 360–365 motif and validate the physiological relevance of its interaction with phospholipids.[34] We used covalently linked single-chain pMHC constructs comprising the KRAS-G12D peptide, β2M, an HA tag, and the full-length HLA-A*11:01 heavy chain, with monomeric teal fluorescent protein (mTFP) fused to the C terminus as the donor. The plasma membrane was labeled with octadecyl rhodamine B (R18), which served as the acceptor. Compared with the Δ360–365 single-chain pMHC construct, the wild-type (WT) construct exhibited

(E) PRE analysis of membrane proximal residues. Signal attenuation (I/I$_0$) for residues L360 and V365 versus distal residues K335 and G342 upon titration with 0–10 mM Gd-DOTA. Minimal PRE attenuation (I/I$_0$ > 0.95 at 10 mM Gd-DOTA) for membrane proximal residues indicates lipid protected positioning. Data acquired at 28°C on an 800 MHz NMR spectrometer.

(F) FRET-based detection of plasma membrane interactions. Confocal microscopy images of WT (left) or Δ360–365 (right) single-chain pMHC constructs labeled with 2 μM octadecyl rhodamine B (R18). FRET efficiency maps (bottom) show reduced membrane association in Δ360-365. Scale bars, 5 μm. BP, before photobleaching; AP, after photobleaching.

(G) Quantification of FRET efficiencies for WT and Δ360–365 single-chain pMHC constructs. Whisker-dot plot comparing FRET efficiencies (WT: n = 21 cells; Δ360–365: n = 29 cells, pooled from 3 independent experiments.). Statistical analyses were performed with the student's t test.

Complete chemical shift assignments and residue specific PRE values are provided in source data. FRET source data provided as source data file.

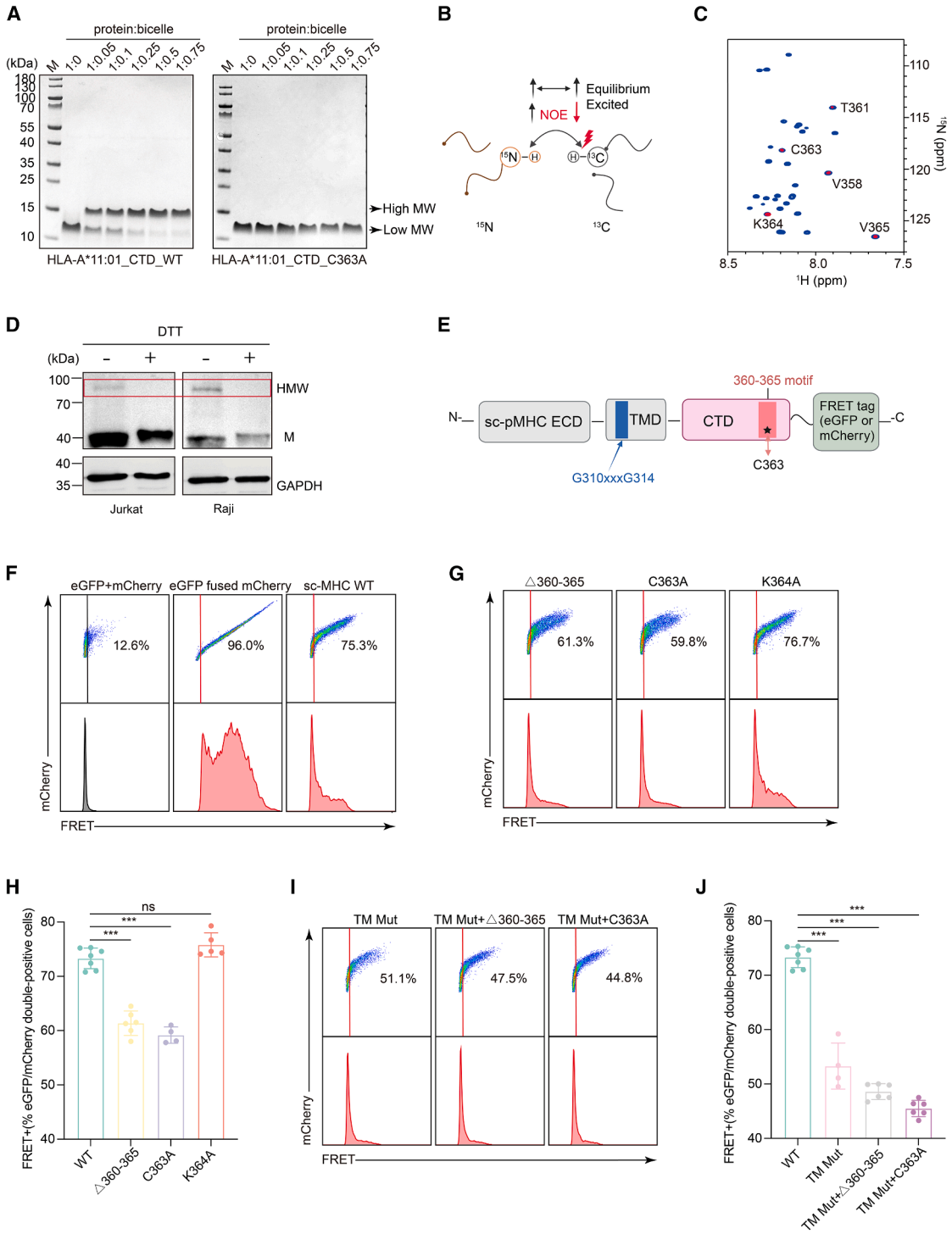


Figure 2. Cys363 and the transmembrane region contribute to HLA-A molecular proximity

(A) Non-reducing SDS-PAGE of WT and C363A HLA-A*11:01 CTD (residues 333–365) in increasing amounts of DMPC/DH_6PC bicelles. The higher molecular weight (HMW) species was reduced by the C363A substitution.

(B) Detection of residue specific inter-chain NOEs using a mixed isotope sample of (^{15}N, ^{2}H)-labeled HLA-A*11:01 CTD and (^{13}C)-labeled HLA-A*11:01 CTD at a 1:1 molar ratio. Two interleaved ^{1}H-^{15}N TROSY-HSQC spectra were recorded at equilibrium and with selective inversion of ^{13}C attached aliphatic protons during a 200 ms NOE-mixing period, yielding an NOE-difference spectrum reporting inter-chain contacts.

(C) Overlay of the NOE-difference spectrum (red) onto the reference ^{1}H-^{15}N TROSY-HSQC spectrum (blue) of the (^{15}N, ^{2}H)-labeled HLA-A*11:01 CTD. Signals in the difference spectrum identify CTD residues exhibiting inter-chain NOEs, with representative residues indicated.

(legend continued on next page)

significantly higher FRET efficiency, indicating that the 360–365 region contributes to HLA-A cytoplasmic tail proximity to the plasma membrane in this cellular system (Figures 1F and 1G). To exclude palmitoylation as a contributing mechanism, we performed acyl-biotin exchange (ABE) assays and detected no palmitoylation in either WT or the C363 mutant (Figure S1F).

By integrating findings from NMR titration, PRE, and live-cell FRET experiments, we conclude that the 360–365 motif directly mediates membrane association in a manner that does not depend on phospholipid charge, distinguishing it from canonical BRS-acidic lipid interactions.[34] This motif therefore represents a previously unrecognized, charge independent module that anchors HLA-A*11:01-CTD to phospholipid bilayers.

Membrane mimetics promote Cys363-dependent association of the HLA-A cytoplasmic tail

Because C363 lies within the DMPC-sensitive 360–365 region, we first asked whether membrane-mimetic engagement alters the association behavior of the isolated HLA-A cytoplasmic tail. When purified HLA-A*11:01 CTD comprising residues 333–365 was incubated with increasing amounts of DMPC/DH_6PC bicelles and analyzed under non-reducing conditions, a higher-molecular-weight species became prominent in the WT sample but was markedly reduced by the C363A substitution (Figure 2A). Alanine substitutions at L360, T361, K364, and V365 produced variable distributions of lower- and higher-molecular-weight species across the bicelle titration series, indicating that residues surrounding C363 do not contribute uniformly to this biochemical behavior (Figure S2A). In parallel, the local chemical environment of C363 was altered in the presence of DMPC bicelles, as indicated by a change in its $^{13}C\beta$ chemical shift (Figure S2B). Together, these observations suggest that membrane-mimetic conditions promote C363-dependent association of the isolated HLA-A*11:01 cytoplasmic tail.

To determine whether this association involved localized inter-chain contacts, we used a mixed isotope NOE-difference NMR approach (Figure 2B). Briefly, (^{15}N, ^{2}H)-labeled CTD was mixed 1:1 with (^{13}C)-labeled CTD and NOE edited spectra were acquired; subtraction from a reference spectrum yielded an NOE difference readout reporting inter-chain contacts. The resulting difference spectrum contained localized signals centered on the membrane-sensitive C-terminal region, including C363 and neighboring residues V358, T361, K364, and V365 (Figure 2C). These data support a specific mode of CTD-CTD association involving the 360–365 region under membrane mimetic conditions.

We next asked whether related HLA-A species could be detected in a cellular context. Under non-reducing conditions, samples prepared from Jurkat and Raji cells contained DTT-sensitive higher-molecular-weight HLA-A immunoreactive species in addition to the monomer-sized heavy chain band (Figure 2D). Because their molecular composition and stoichiometry were not established, these species were not assigned as discrete native peptide-β2M-HLA-A dimers. To examine whether the cytoplasmic tail region also contributes to molecular proximity in a membrane embedded context, we established a flow cytometry-based FRET assay using covalently linked single-chain pMHC constructs comprising the G12D peptide, β2M, and the full-length HLA-A*11:01 heavy chain, with either eGFP or mCherry fused to the C terminus of the cytoplasmic tail (Figure 2E). Co-expression of unfused eGFP and mCherry produced a low FRET background, whereas a directly fused eGFP-mCherry construct yielded a high FRET positive fraction, defining the dynamic range of the assay (Figure 2F). The WT single-chain pMHC construct showed a robust FRET signal, whereas deletion of residues 360–365 or substitution of C363 significantly reduced the FRET positive fraction (Figures 2G and 2H). In contrast, K364A remained comparable to WT. Additional substitutions at V358, T361, and V365 likewise did not significantly alter the FRET-positive fraction under the tested conditions (Figures S2C and S2D). These results indicate that the C363 containing cytoplasmic tail region contributes to relative molecular proximity in the single-chain pMHC system, whereas substitutions at several neighboring residues do not uniformly affect this readout.

Substantial FRET nevertheless remained in the Δ360–365 and C363A variants, indicating that the cytoplasmic tail was not the sole determinant of proximity in this assay. The HLA-A*11:01 transmembrane region contains a G310xxxG314 sequence that could contribute to transmembrane helix packing. We therefore introduced a G310L/G314L double substitution, hereafter referred to as TM-mut, to perturb this sequence. TM-mut, TM-mut + Δ360-365, and TM-mut + C363A all showed significantly lower FRET-positive fractions than WT (Figures 2I and 2J). Thus, the transmembrane region provides an additional contribution to the molecular proximity measured in the single-chain pMHC system. Together, these findings support a model in

(D) Immunoblot detection of DTT-sensitive higher molecular weight HLA-A species in samples prepared from Jurkat and Raji cells. Samples were analyzed under non-reducing conditions in the absence or presence of 10 mM DTT. HMW, higher-molecular-weight HLA-A species; M, monomer-sized HLA-A species.
(E) Schematic of the covalently linked single-chain pMHC FRET constructs comprising the G12D peptide, β2M, and full-length HLA-A*11:01 heavy chain, followed by a C-terminal eGFP or mCherry tag. The HLA-A transmembrane G310xxxG314 sequence, G310L/G314L TM mutant, cytoplasmic tail residues 360–365, and C363 are indicated.
(F) Representative flow cytometry-based FRET plots for cells co-expressing unfused eGFP and mCherry, a directly fused eGFP-mCherry positive control, or WT single-chain pMHC -eGFP and –mCherry constructs.
(G) Representative FRET plots for the Δ360–365, C363A, and K364A single-chain pMHC variants.
(H) Quantification of the FRET-positive fraction among eGFP/mCherry double-positive cells expressing WT, Δ360–365, C363A, or K364A constructs.
(I) Representative FRET plots for the G310L/G314L transmembrane mutant (TM-mut), TM-mut + Δ360–365, and TM-mut + C363A constructs.
(J) Quantification of the FRET-positive fraction for WT, TM-mut, TM-mut + Δ360–365, and TM-mut + C363A constructs.
Data in (H) and (J) are presented as mean ± SD, with each point representing an independent experiment. In (H), $n = 7$, 6, 4, and 5 for WT, Δ360–365, C363A, and K364A, respectively. In (J), $n = 7$, 4, 6, and 6 for WT, TM-mut, TM-mut + Δ360-365, and TM-mut + C363A, respectively. Statistical significance was determined using ordinary one-way ANOVA followed by Dunnett's multiple-comparisons test, with WT as the control. $^{***}p < 0.001$; ns, not significant. Exact p values are provided in the source data. See also Figure S2.

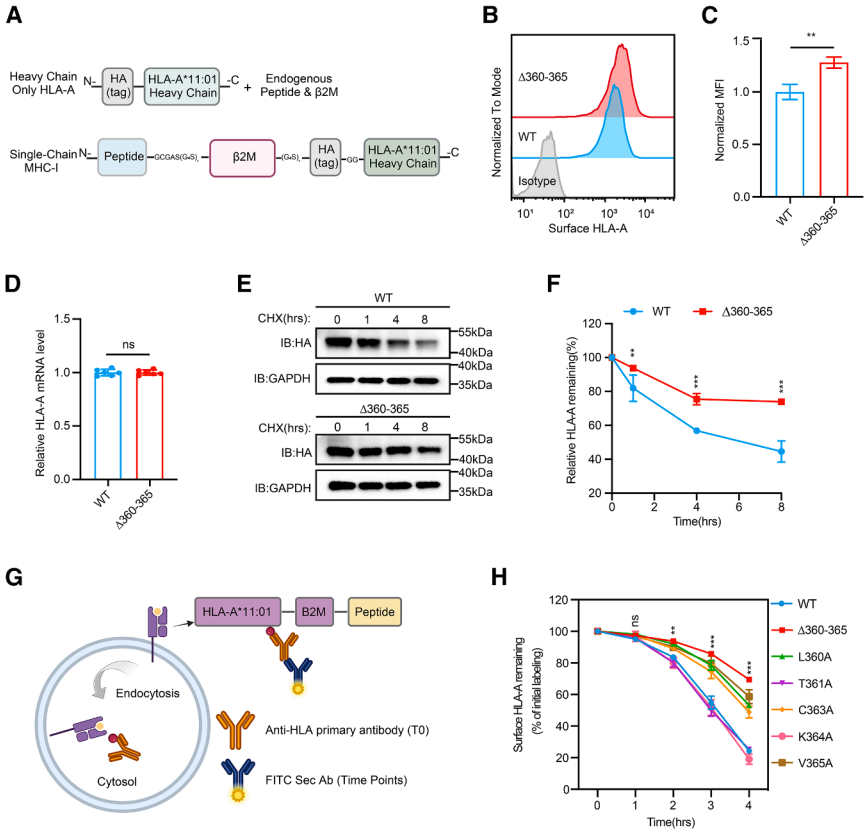


Figure 3. The HLA-A 360–365 region promotes internalization and limits surface retention

(A) Schematics of the HLA-A*11:01 constructs used in the cellular assays. The N-terminally HA-tagged heavy-chain-only HLA-A construct assembles non-covalently with endogenous β2M and cellular peptides. In the engineered single-chain pMHC construct, the peptide, β2M, HA tag, and full-length HLA-A*11:01 heavy chain are connected through flexible linkers.

(B and C) Surface abundance of heavy-chain-only HLA-A*11:01 in pooled stable MCF7 populations expressing WT or Δ360–365 constructs. Representative flow cytometry histograms are shown in (B), with the isotype control shown in gray. Normalized mean fluorescence intensity (MFI) is quantified in (C), with the WT mean set to 1.

(D) qRT-PCR analysis of HLA-A transcript levels in pooled stable MCF7 populations expressing WT or Δ360–365 heavy-chain-only constructs. HLA-A transcript abundance was normalized to GAPDH.

(E and F) Cycloheximide-chase analysis of heavy-chain-only HLA-A*11:01 in pooled stable 293T populations. Cells expressing WT or Δ360–365 constructs were treated with 100 μg/mL cycloheximide (CHX) for the indicated times. Representative immunoblots for HA-tagged HLA-A and GAPDH are shown in (E). HLA-A abundance was normalized to GAPDH and then to the corresponding signal at 0 h (F).

(G) Schematic of the surface pre-labeling internalization assay. Surface exposed HLA-A was labeled with an anti-HA primary antibody at 4°C, after which cells were transferred to 37°C to allow internalization. At the indicated time points, the fraction of the initially labeled HLA-A pool that remained accessible at the cell surface was detected using an FITC-conjugated anti-mouse secondary antibody.

(H) Internalization profiles of heavy-chain-only WT, Δ360–365, L360A, T361A, C363A, K364A, and V365A HLA-A*11:01 constructs in pooled stable MCF7 populations. Surface accessible fluorescence at each time point was normalized to the corresponding value at 0 h for each construct.

Data are presented as mean ± SD. In (C), (F), and (H), $n = 3$ independent experiments; in (D), $n = 6$ independent experiments. Statistical significance in (C) and (D) was determined using an unpaired two-tailed student's t test. Statistical significance in (F) and (H) was determined using two-way ANOVA followed by Dunnett's multiple-comparisons test. Statistical annotations in (H) indicate comparisons between WT and Δ360–365 at each time point. $^{**}p < 0.01$, $^{***}p < 0.001$; ns, not significant. Exact p values are provided in the source data. See also Figure S3.

which membrane engagement promotes C363-dependent association of the HLA-A cytoplasmic tail, with the transmembrane region providing an additional contribution to molecular proximity.

The HLA-A 360–365 region promotes internalization and limits surface retention

Having established that the 360–365 region contributes to membrane engagement and to the relative proximity of full-length HLA-A molecules, we next asked whether this cytoplasmic tail motif regulates HLA-A surface stability and internalization in a cellular context. We generated N-terminally HA-tagged, heavy-chain-only HLA-A*11:01 constructs, allowing the heavy chain to assemble noncovalently with endogenous β2M and cellular peptides (Figure 3A). In pooled MCF7 populations expressing WT or Δ360–365 HLA-A*11:01, deletion of residues 360–365 significantly increased the abundance of HLA-A at the cell surface (Figures 3B and 3C). HLA-A transcript levels were

comparable between WT and Δ360–365 cells (Figure 3D), indicating that the elevated surface abundance was not explained by increased transcription. The same directional effect was observed in an engineered covalently linked single-chain pMHC system, in which Δ360–365 increased surface abundance without altering HLA-A transcript levels (Figure 3A; Figures S3A–S3C).

We next examined whether the increased surface abundance of Δ360–365 was accompanied by altered protein turnover. Following inhibition of *de novo* protein synthesis with cycloheximide, WT heavy-chain-only HLA-A progressively declined during the 8-h time course, whereas the Δ360–365 construct was retained to a greater extent (Figures 3E and 3F). The engineered single-chain pMHC construct carrying Δ360–365 similarly showed slower protein loss than WT during cycloheximide treatment (Figures S3D and S3E). These results indicate that deletion of the 360–365 region slows HLA-A protein turnover.

We next asked whether the increased surface retention and slower turnover of Δ360–365 HLA-A were associated with altered internalization from the plasma membrane. To directly follow the fate of a defined surface HLA-A pool, we established an antibody-based surface pre-labeling assay. Cells were first incubated with an anti-HA primary antibody at 4°C, a condition that permits labeling of surface exposed HLA-A while minimizing membrane trafficking. After removal of unbound antibody, the cells were transferred to 37°C to allow internalization to proceed. At the indicated time points, cells were returned to 4°C and stained with a fluorescent secondary antibody, which detected the fraction of the initially labeled HLA-A pool that remained accessible at the extracellular surface (Figure 3G). Surface associated fluorescence at each time point was normalized to the corresponding signal at time zero, thereby allowing the loss of the pre-labeled surface pool to be followed independently of differences in initial surface abundance.

WT HLA-A showed a progressive reduction in surface accessible label over time, consistent with continuous removal of the pre-labeled HLA-A pool from the plasma membrane. In contrast, Δ360–365 retained a substantially larger fraction of the initial surface associated signal throughout the time course, indicating slower loss of HLA-A from the cell surface and supporting reduced internalization (Figure 3H). Representative flow cytometry plots corresponding to this analysis are shown in Figure S3F. We further examined individual substitutions within the 360–365 region. L360A, C363A, and V365A produced intermediate retention of the surface labeled HLA-A pool, whereas T361A and K364A more closely followed the WT profile (Figure 3H). Thus, although deletion of the complete region produced the strongest phenotype, individual residues within the motif contributed to HLA-A internalization to different extents.

Reduced internalization of Δ360–365 was also observed in the engineered covalently linked single-chain pMHC system, and C363A and V365A produced effects in the same direction (Figures S3G and S3H). The magnitude of the phenotypes caused by individual substitutions was not identical between the heavy-chain-only and single-chain pMHC constructs, particularly for L360A, indicating that residue level contributions can vary with construct context. Nevertheless, the consistent effect of deleting the complete 360–365 region across the two systems supports a central role for this cytoplasmic tail segment in promoting HLA-A internalization. Together, these results indicate that the 360–365 region facilitates removal of HLA-A from the plasma membrane and accelerates protein turnover, thereby limiting HLA-A retention at the cell surface.

The HLA-A 360–365 region regulates ARF6-associated trafficking

Having found that deletion of the 360–365 region slows HLA-A internalization, we next sought to identify trafficking factors associated with HLA-A. Immunoprecipitation followed by mass spectrometry identified multiple proteins involved in membrane trafficking, including clathrin-adaptor components, small GTPases, and vesicular transport regulators (Figure 4A). Among these candidates, we focused on ARF6 because of its previously reported involvement in HLA-I trafficking.[22,31,39–43]

We first examined whether the 360–365 region contributes to the cellular association between HLA-A and endogenous ARF6. HA-tagged heavy-chain-only WT or Δ360–365 HLA-A*11:01 constructs were expressed in A549 and PANC-1 cells and subjected to anti-HA immunoprecipitation. Endogenous ARF6 co-immunoprecipitated with WT HLA-A in both cell types, whereas substantially less ARF6 was recovered with the Δ360–365 construct (Figures 4B and 4C). Comparable directional effects were also observed in 293T and A549 cells expressing engineered covalently linked single-chain pMHC constructs, in which deletion of residues 360–365 reduced the amount of ARF6 detected in the HA immunoprecipitates (Figures S4A and S4B). These results indicate that the 360–365 region contributes to the cellular association of HLA-A with ARF6 across different construct and cellular contexts.

We next asked whether this altered association was accompanied by a change in the responsiveness of surface HLA-A to increased ARF6 expression. In 293T cells expressing the covalently linked single-chain pMHC constructs, ARF6 overexpression significantly reduced the surface abundance of WT pMHC (Figure 4D). In contrast, surface abundance of the Δ360–365 construct was not significantly altered by ARF6 overexpression (Figure 4E). Thus, deletion of the 360–365 region rendered surface HLA-A comparatively insensitive to increased ARF6 expression, linking this cytoplasmic tail region to ARF6-responsive surface regulation.

To assess whether the 360–365 region also influenced the proximity of ARF6 to the plasma membrane, we performed acceptor-photobleaching FRET using ARF6–TFP as the donor and the plasma-membrane dye R18 as the acceptor. Cells expressing WT single-chain pMHC showed substantial donor dequenching following R18 photobleaching, whereas markedly lower FRET efficiencies were observed in cells expressing the Δ360–365 construct (Figures 4F and 4G). These findings indicate that the presence of the 360–365 region is associated with greater ARF6 proximity to the plasma membrane under the tested conditions. Together, the co-immunoprecipitation, surface-abundance, and FRET results support a model in which the HLA-A 360–365 region contributes to ARF6 association and enables ARF6-responsive regulation of HLA-A surface abundance.

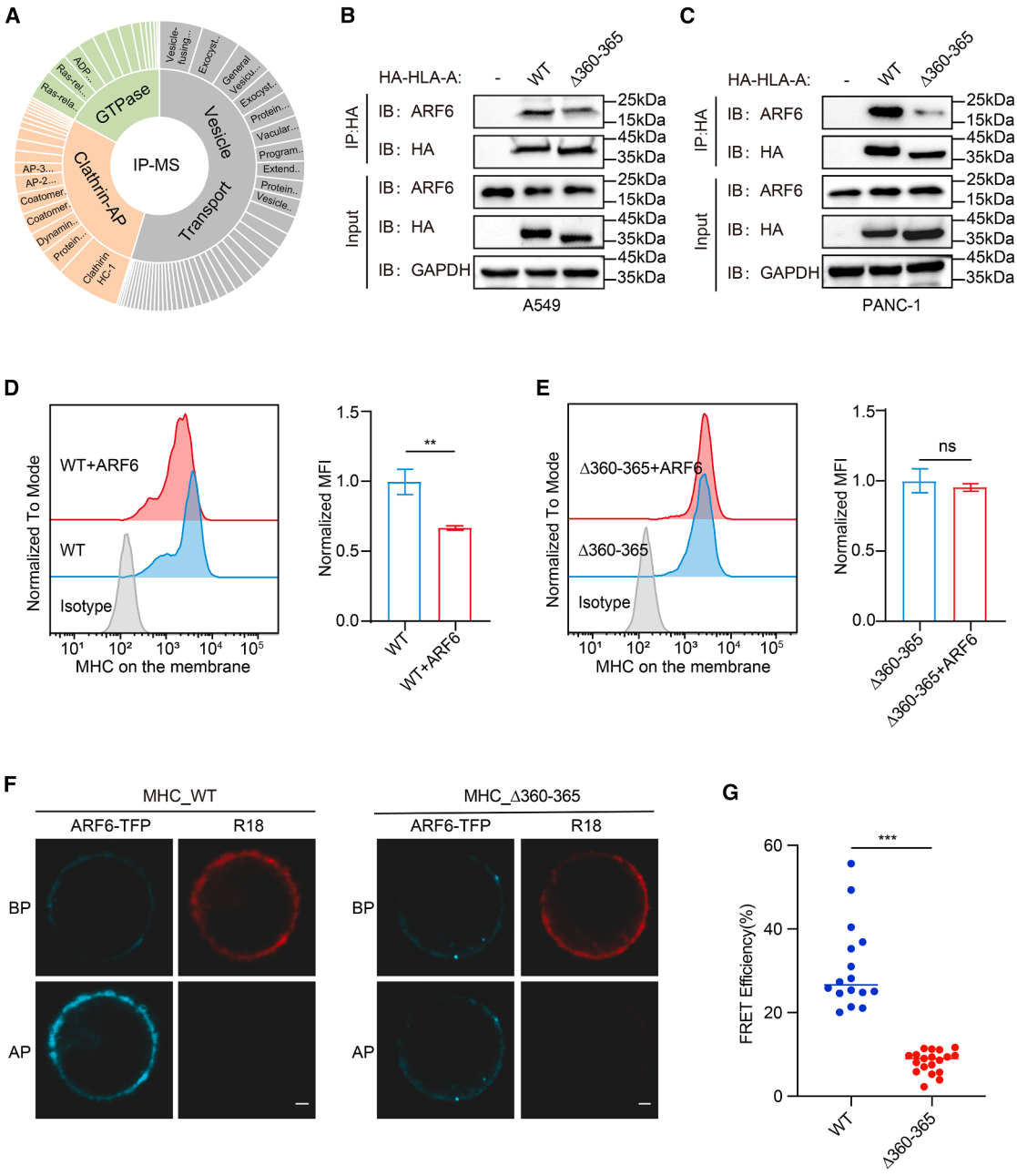


Figure 4. The HLA-A 360–365 region regulates ARF6-associated trafficking

(A) IP-MS analysis of proteins associated with HA-tagged HLA-A complexes isolated from 293T cells. Trafficking related proteins are grouped as clathrin-adaptor components, small GTPases, and vesicular transport regulators.

(B and C) Co-immunoprecipitation of endogenous ARF6 with heavy-chain-only WT or Δ360–365 HLA-A*11:01 in A549 (B) and PANC-1 (C) cells. Cells expressing no HA-tagged construct (–) were included as controls. Immunoprecipitated and input fractions were analyzed by immunoblotting for ARF6 and HA; GAPDH served as an input loading control.

(D and E) Surface abundance of covalently linked single-chain pMHC constructs in monoclonal 293T cells following ARF6 overexpression. Representative flow cytometry histograms and normalized MFI are shown for WT (D) and Δ360–365 (E). For each construct, the mean MFI without ARF6 overexpression was set to 1.

(F and G) Acceptor-photobleaching FRET analysis of ARF6 proximity to the plasma membrane in 293T cells expressing WT or Δ360–365 single-chain pMHC. ARF6-TFP was the donor and R18 was the membrane-localized acceptor. Representative images before and after photobleaching are shown in (F), and FRET efficiencies are quantified in (G). BP, before photobleaching; AP, after photobleaching. Scale bars, 2 μm.

Data in (D) and (E) are mean ± SD from three independent experiments. In (G), each point represents one cell (WT, $n = 16$; Δ360-365, $n = 19$; pooled from 3 independent experiments), and horizontal lines indicate the mean. Statistical significance was determined using an unpaired two-tailed student's t test. $^{**}p < 0.01$, $^{***}p < 0.001$; ns, not significant. See also Figure S4.

A cell penetrating HLA-A cytoplasmic tail peptide promotes HLA-I surface retention

Having established that the HLA-A 360–365 region regulates internalization and is linked to ARF6-associated trafficking, we asked whether a synthetic cytoplasmic tail peptide could modulate HLA-I surface dynamics. We designed a series of peptides based on the cell penetrating sequence HLYVSPWGG. CPP-WT contained an HLA-A exon 7 derived cytoplasmic tail sequence encompassing residues 360–365, whereas CPP-C363A carried a single C363A substitution within the same sequence. CPP alone and CPP fused to a length-matched irrelevant sequence, designated CPP-irrelevant, were included to control for effects of the cell penetrating moiety and nonspecific peptide fusion, respectively.

We first examined whether these peptides altered HLA-A protein turnover. HA-tagged heavy-chain-only HLA-A*11:01 expressed in 293T cells was monitored by cycloheximide chase in the presence of 10 μM peptide. In the DMSO, CPP, and CPP-irrelevant groups, HA-tagged HLA-A progressively declined over the 8-h time course. By contrast, substantially more HLA-A was retained in cells treated with CPP-WT, resulting in a significantly slower loss of protein across the complete time course (Figures 5A and 5B). CPP-C363A produced an intermediate profile and was less effective than CPP-WT, indicating that C363 contributes substantially to the stabilizing activity of the cytoplasmic tail peptide. Thus, the WT HLA-A tail sequence, rather than the CPP moiety alone, slows HLA-A protein turnover.

Because increased total protein abundance does not necessarily indicate altered surface trafficking, we next followed the fate of a defined pool of endogenous surface HLA-I in Raji cells. Surface HLA-I complexes were pre-labeled with the conformation sensitive W6/32 antibody at 4°C, after which cells were transferred to 37°C in the presence of 1 μM peptide. The fraction of the initially labeled HLA-I pool that remained accessible at the cell surface was quantified over time. DMSO-, CPP-, and CPP-irrelevant treated cells showed a progressive and largely comparable loss of surface-associated label. In contrast, CPP-WT maintained a substantially larger fraction of the pre-labeled HLA-I pool throughout the 120-min time course, consistent with slower internalization and enhanced surface retention (Figure 5C; Figure S5A). CPP-C363A again showed a weaker, intermediate effect. Consistent with these kinetic measurements, CPP-WT significantly increased steady-state surface HLA-I abundance in Raji cells, whereas CPP, CPP-C363A, and CPP-irrelevant produced substantially smaller effects (Figures 5D and 5E).

We then examined whether this activity extended beyond the Raji cell background. Treatment with CPP-WT increased endogenous surface HLA-I abundance in both A549 and PANC-1 cells at peptide concentrations of 10 μM and 5 μM, respectively, whereas the control peptides produced little or no comparable increase (Figures 5F–5I). Surface pre-labeling analyses in these cells yielded the same overall pattern: CPP-WT delayed the loss of the initially labeled surface HLA-I pool, while CPP, CPP-irrelevant, and CPP-C363A showed markedly weaker effects (Figures S5B–S5E). Although the residual activity of CPP-C363A varied among cell types, its consistently reduced effect relative to CPP-WT further supports an important contribution of C363 to peptide function.

Together, these findings show that a cell penetrating HLA-A cytoplasmic tail peptide containing the 360–365 region slows HLA-A protein turnover and promotes endogenous HLA-I surface retention across multiple tumor cell contexts. The reproducible activity of CPP-WT, together with its attenuation by the C363A substitution, identifies the 360–365 containing tail sequence as a transferable modulator of HLA-I surface dynamics.

DISCUSSION

The surface lifetime of HLA class I molecules is generally considered to emerge from the combined effects of biosynthesis, peptide loading, endosomal recycling, and intracellular degradation. Our findings add a receptor-intrinsic layer to this framework by identifying the HLA-A cytoplasmic tail as an active determinant of surface trafficking. Rather than functioning as a passive connection between the transmembrane helix and the cytosol, the C-terminal 360–365 region responds to the membrane environment and biases HLA-A toward internalization rather than prolonged surface retention. This concept helps connect the molecular organization of a short cytoplasmic sequence to the availability of assembled HLA-I complexes at the plasma membrane. Because surface HLA-I is the substrate for both immune recognition and subsequent intracellular sorting, regulation at this proximal step could influence receptor abundance before downstream recycling or degradative pathways become engaged.

The biophysical data favor a dynamic and multicomponent organization of HLA-A over a single, fixed oligomeric state. Previous studies of CD3ε, CD28, and PD-L1 established that short immune receptor cytoplasmic domains can associate with membranes through electrostatic interactions between basic residues and anionic phospholipids.[34,35] The HLA-A tail appears to extend this paradigm. Its membrane proximal basic region responds to anionic lipids, whereas the distal 360–365 segment is also sensitive to a zwitterionic membrane mimetic environment. C363 dependent association of the isolated tail may therefore represent a membrane favored arrangement of this distal segment, rather than an obligatory native HLA-A dimer. This interpretation is consistent with the unresolved composition of the higher-molecular-weight cellular species and with the persistence of substantial full-length FRET after disruption of the cytoplasmic tail region. The additional effect of the transmembrane mutation further suggests that molecular proximity is distributed across the membrane spanning and cytoplasmic portions of HLA-A. Membrane engagement, transmembrane packing, and local tail association may thus cooperate to generate an ensemble of receptor states with different trafficking properties.

The functional significance of this membrane sensitive organization is reflected in HLA-A trafficking. Deletion of residues 360–365 prolonged surface retention and slowed protein turnover, indicating that the cytoplasmic tail helps regulate HLA-A exit from the plasma membrane. ARF6 appears to participate in this process, as the deletion weakened HLA-A-ARF6 association and altered both ARF6 membrane proximity and the response of

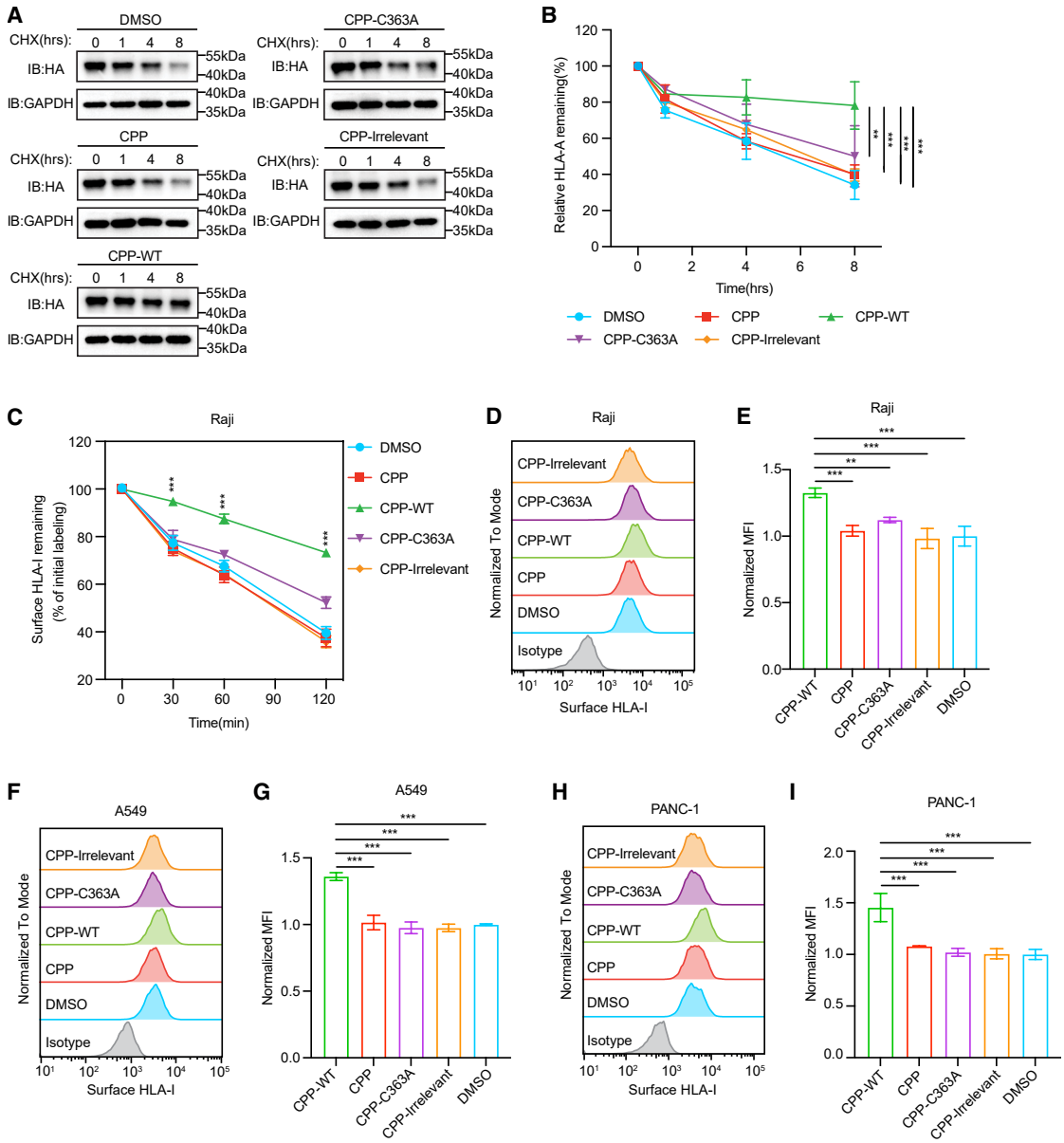


Figure 5. A cell-penetrating HLA-A cytoplasmic-tail peptide promotes HLA-I surface retention

CPP-WT contains a cell penetrating sequence fused to an HLA-A exon 7 derived sequence encompassing residues 360–365. CPP-C363A carries the corresponding C363A substitution. CPP alone and CPP-irrelevant were included as controls.

(A and B) Cycloheximide-chase analysis of HA-tagged heavy-chain-only HLA-A*11:01 in 293T cells treated with DMSO or 10 μM peptides. Representative immunoblots are shown in (A). HLA-A abundance was normalized to GAPDH and the corresponding 0-h value in (B).

(C) Retention of pre-labeled surface HLA-I in Raji cells treated with DMSO or 1 μM peptide. Each group was normalized to its corresponding 0-min value.

(D and E) Representative flow cytometry histograms (D) and normalized surface HLA-I MFI (E) in Raji cells following treatment with DMSO or 1 μM peptide.

(F and G) Representative histograms (F) and normalized surface HLA-I MFI (G) in A549 cells treated with DMSO or 10 μM peptides.

(H and I) Representative histograms (H) and normalized surface HLA-I MFI (I) in PANC-1 cells treated with DMSO or 5 μM peptides.

Data are mean ± SD from three independent experiments. Statistical significance in (B) was determined using two-way ANOVA followed by Dunnett's multiple-comparisons test, with CPP-WT as the reference group. Annotations represent overall comparisons across the complete time course and, from left to right, correspond to CPP-C363A, CPP, CPP-irrelevant, and DMSO versus CPP-WT. Statistical significance in (C) was determined using two-way ANOVA followed by Dunnett's multiple-comparisons test. Statistical annotations indicate comparisons between DMSO and CPP-WT at each indicated time point. Statistical significance in (E), (G), and (I) was determined using ordinary one-way ANOVA followed by Dunnett's multiple-comparisons test, with CPP-WT as the reference group. $^{**}p < 0.01$, $^{***}p < 0.001$.

surface HLA-A to ARF6 overexpression. Together with the broader set of trafficking proteins identified by IP-MS, these findings support a model in which membrane engagement of the HLA-A tail modulates access to an interconnected trafficking network that includes ARF6. The peptide experiments further indicate that regulatory information within the HLA-A tail is functionally transferable. CPP-WT promoted HLA-I surface retention across several tumor cell lines, whereas CPP alone and CPP-irrelevant showed little comparable activity. The weaker effect of CPP-C363A supports an important contribution of C363 while also suggesting that the broader tail sequence is required. Thus, CPP-WT complements the genetic deletion studies by showing that a tail derived sequence can modulate HLA-I trafficking in trans. More broadly, these findings identify the HLA-A cytoplasmic tail as a regulatory interface linking membrane organization to the surface lifetime of antigen presenting complexes.

Limitations of the study

Several limitations should be considered when interpreting these findings. First, the mechanistic analyses focused primarily on HLA-A*11:01 and frequently used ectopically expressed constructs in transformed cell lines. Whether the same membrane-responsive mechanism operates at endogenous expression levels, in primary cells, or across other HLA-A, HLA-B, and HLA-C allotypes remains to be determined. Second, self-association of the isolated cytoplasmic tail in bicelles and FRET between full-length constructs report membrane-associated proximity but do not establish the existence, stoichiometry, lifetime, or high-resolution structure of a discrete native HLA-A oligomer. Third, the surface pre-labeling assay measures the net loss of an initially labeled receptor pool from the extracellular surface and therefore cannot fully distinguish altered internalization from changes in recycling, intracellular sorting, or degradation. Fourth, the current ARF6 experiments demonstrate association and responsiveness but not direct binding or a requirement for endogenous ARF6. Addressing these questions will be necessary to define the generality and physiological significance of this cytoplasmic tail regulatory mechanism.

RESOURCE AVAILABILITY

Lead contact

Further information and requests for resources and reagents should be directed to and will be fulfilled by the lead contact, Linlin Zhao (lzhao@tongji.edu.cn).

Materials availability

Plasmid constructs and other unique reagents generated in this study are available from the lead contact upon reasonable request and with a completed Materials Transfer Agreement, where applicable.

Data and code availability

- All data supporting the conclusions of this study are included in the study and its supplemental information. Additional raw data, including NMR spectra, flow cytometry data, microscopy data, and original immunoblot images, are available from the lead contact upon reasonable request.
- This study does not report original code.
- Any additional information required to reanalyze the data reported in this study is available from the lead contact upon request.

ACKNOWLEDGMENTS

We thank the staff members of the Nuclear Magnetic Resonance System (https://cstr.cn/31129.02.NFPS.NMRSystem) at the National Facility for Protein Science in Shanghai (https://cstr.cn/31129.02.NFPS), for providing technical support and assistance in data collection and analysis. We thank Pro. Lan Fang, Pro. Jian Yuan, Pro. Jian Luo, and Pro Minjia Tan at Cancer Research Center Tongji Medical School for discussion assistance regarding the study. This work was supported by the National Natural Science Foundation of China (32301027, 32571410 to L.Z.; 82350710799 to J.J.C. and L.Z.), the Shanghai Health Commission Clinical Research Special Youth Project (2022YQ079 to L.Z.), the Science and Technology Commission of Shanghai Municipality (22JC1410500 to J.J.C.), the Strategic Priority Research Program of the Chinese Academy of Sciences (XDB1060000 to J.J.C.), and the Shanghai Basic Research Pioneer Project and the Shanghai Municipal Science and Technology Major Project (both to J.J.C.).

AUTHOR CONTRIBUTIONS

Conceptualization, L.Z.; methodology, X.X., Z. Chen, J.J.C., and L.Z.; investigation, X.X., Y. Wang, H.W., M.W., J.Z., Z. Cai, J.L., H.X., and Y. Wu; formal analysis, X.X. and Y. Wang; visualization, X.X. and Y. Wu; writing – original draft, L.Z.; writing – review and editing, J.J.C., Z. Chen, and L.Z.; supervision, L.Z.

DECLARATION OF INTERESTS

The authors declare no competing interests.

STAR★METHODS

Detailed methods are provided in the online version of this paper and include the following:

- KEY RESOURCES TABLE
- EXPERIMENTAL MODEL AND STUDY PARTICIPANT DETAILS
  - Cell lines and culture conditions
- METHOD DETAILS
  - Plasmid construction and mutagenesis
  - Protein expression and purification
  - Preparation of bicelle associated HLA-A-CTD for NMR measurements
  - Assignment of NMR resonances
  - Characterization of HLA-A-CTD membrane interaction using paramagnetic probe titration
  - Assignment of NOE restraints
  - Quantitative measurement of fluorescence resonance energy transfer (FRET)
  - Non-reducing SDS-PAGE analysis of purified HLA-A*11:01 CTD
  - Flow cytometry analysis
  - Western blot
  - qRT-PCR analysis
- QUANTIFICATION AND STATISTICAL ANALYSIS

SUPPLEMENTAL INFORMATION

Supplemental information can be found online at https://doi.org/10.1016/j.celrep.2026.117940.

Received: February 24, 2026
Revised: July 20, 2026
Accepted: August 18, 2026
Published: September 3, 2026

REFERENCES

1. Dersh, D., Hollý, J., and Yewdell, J.W. (2021). A few good peptides: MHC class I-based cancer immunosurveillance and immunoevasion. Nat. Rev. Immunol. *21*, 116–128. https://doi.org/10.1038/s41577-020-0390-6.
2. Waddell, N., Pajic, M., Patch, A.M., Chang, D.K., Kassahn, K.S., Bailey, P., Johns, A.L., Miller, D., Nones, K., Quek, K., et al. (2015). Whole genomes redefine the mutational landscape of pancreatic cancer. Nature *518*, 495–501. https://doi.org/10.1038/nature14169.
3. McGranahan, N., Rosenthal, R., Hiley, C.T., Rowan, A.J., Watkins, T.B.K., Wilson, G.A., Birkbak, N.J., Veeriah, S., Van Loo, P., Herrero, J., et al. (2017). Allele-Specific HLA Loss and Immune Escape in Lung Cancer Evolution. Cell *171*, 1259–1271.e11. https://doi.org/10.1016/j.cell.2017.10.001.
4. Gettinger, S., Choi, J., Hastings, K., Truini, A., Datar, I., Sowell, R., Wurtz, A., Dong, W., Cai, G., Melnick, M.A., et al. (2017). Impaired HLA Class I Antigen Processing and Presentation as a Mechanism of Acquired Resistance to Immune Checkpoint Inhibitors in Lung Cancer. Cancer Discov. *7*, 1420–1435. https://doi.org/10.1158/2159-8290.CD-17-0593.
5. Pandha, H., Rigg, A., John, J., and Lemoine, N. (2007). Loss of expression of antigen-presenting molecules in human pancreatic cancer and pancreatic cancer cell lines. Clin. Exp. Immunol. *148*, 127–135. https://doi.org/10.1111/j.1365-2249.2006.03289.x.
6. Schrörs, B., Lübcke, S., Lennerz, V., Fatho, M., Bicker, A., Wölfel, C., Derigs, P., Hankeln, T., Schadendorf, D., Paschen, A., and Wölfel, T. (2017). HLA class I loss in metachronous metastases prevents continuous T cell recognition of mutated neoantigens in a human melanoma model. Oncotarget *8*, 28312–28327. https://doi.org/10.18632/oncotarget.16048.
7. Taylor, B.C., Sun, X., Gonzalez-Ericsson, P.I., Sanchez, V., Sanders, M.E., Wescott, E.C., Opalenik, S.R., Hanna, A., Chou, S.T., Van Kaer, L., et al. (2024). NKG2A Is a Therapeutic Vulnerability in Immunotherapy Resistant MHC-I Heterogeneous Triple-Negative Breast Cancer. Cancer Discov. *14*, 290–307. https://doi.org/10.1158/2159-8290.CD-23-0519.
8. Anderson, P., Aptsiauri, N., Ruiz-Cabello, F., and Garrido, F. (2021). HLA class I loss in colorectal cancer: implications for immune escape and immunotherapy. Cell. Mol. Immunol. *18*, 556–565. https://doi.org/10.1038/s41423-021-00634-7.
9. Hanalioglu, D., Ayvaz, D.C., Ozgur, T.T., van der Burg, M., Sanal, O., and Tezcan, I. (2017). A novel mutation in TAP1 gene leading to MHC class I deficiency: Report of two cases and review of the literature. Clin. Immunol. *178*, 74–78. https://doi.org/10.1016/j.clim.2017.01.011.
10. Bradley, C.A. (2019). PRC2-mediated MHC-I silencing drives immune evasion. Nat. Rev. Cancer *19*, 664. https://doi.org/10.1038/s41568-019-0219-4.
11. Tovar Perez, J.E., Zhang, S., Hodgeman, W., Kapoor, S., Rajendran, P., Kobayashi, K.S., and Dashwood, R.H. (2024). Epigenetic regulation of major histocompatibility complexes in gastrointestinal malignancies and the potential for clinical interception. Clin. Epigenetics *16*, 83. https://doi.org/10.1186/s13148-024-01698-8.
12. Li, X., Yi, H., Jin, Z., Jiang, K., Xue, K., Wang, J., Qian, Y., Xiang, Q., Zhu, S., Yan, R., et al. (2024). MCRS1 sensitizes T cell-dependent immunotherapy by augmenting MHC-I expression in solid tumors. J. Exp. Med. *221*, e20240959. https://doi.org/10.1084/jem.20240959.
13. Yamamoto, K., Venida, A., Yano, J., Biancur, D.E., Kakiuchi, M., Gupta, S., Sohn, A.S.W., Mukhopadhyay, S., Lin, E.Y., Parker, S.J., et al. (2020). Autophagy promotes immune evasion of pancreatic cancer by degrading MHC-I. Nature *581*, 100–105. https://doi.org/10.1038/s41586-020-2229-5.
14. Herhaus, L., Gestal-Mato, U., Eapen, V.V., Mačinković, I., Bailey, H.J., Prieto-Garcia, C., Misra, M., Jacomin, A.C., Ammanath, A.V., Bagarić, I., et al. (2024). IRGQ-mediated autophagy in MHC class I quality control promotes tumor immune evasion. Cell *187*, 7285–7302.e29. https://doi.org/10.1016/j.cell.2024.09.048.
15. Deng, Y., Xia, X., Zhao, Y., Zhao, Z., Martinez, C., Yin, W., Yao, J., Hang, Q., Wu, W., Zhang, J., et al. (2021). Glucocorticoid receptor regulates PD-L1 and MHC-I in pancreatic cancer cells to promote immune evasion and immunotherapy resistance. Nat. Commun. *12*, 7041. https://doi.org/10.1038/s41467-021-27349-7.
16. Lin, W., Chen, L., Zhang, H., Qiu, X., Huang, Q., Wan, F., Le, Z., Geng, S., Zhang, A., Qiu, S., et al. (2023). Tumor-intrinsic YTHDF1 drives immune evasion and resistance to immune checkpoint inhibitors via promoting MHC-I degradation. Nat. Commun. *14*, 265. https://doi.org/10.1038/s41467-022-35710-7.
17. Yu, Q., Dong, Y., Wang, X., Su, C., Zhang, R., Xu, W., Jiang, S., Dang, Y., and Jiang, W. (2024). Pharmacological induction of MHC-I expression in tumor cells revitalizes T cell antitumor immunity. JCI Insight *9*, e177788. https://doi.org/10.1172/jci.insight.177788.
18. Sang, W., Zhou, Y., Chen, H., Yu, C., Dai, L., Liu, Z., Chen, L., Fang, Y., Ma, P., Wu, X., et al. (2024). Receptor-interacting Protein Kinase 2 Is an Immunotherapy Target in Pancreatic Cancer. Cancer Discov. *14*, 326–347. https://doi.org/10.1158/2159-8290.CD-23-0584.
19. Chen, X., Lu, Q., Zhou, H., Liu, J., Nadorp, B., Lasry, A., Sun, Z., Lai, B., Rona, G., Zhang, J., et al. (2023). A membrane-associated MHC-I inhibitory axis for cancer immune evasion. Cell *186*, 3903–3920.e21. https://doi.org/10.1016/j.cell.2023.07.016.
20. Cebrian, I., Croce, C., Guerrero, N.A., Blanchard, N., and Mayorga, L.S. (2016). Rab22a controls MHC-I intracellular trafficking and antigen cross-presentation by dendritic cells. EMBO Rep. *17*, 1753–1765. https://doi.org/10.15252/embr.201642358.
21. Olson, E., Ceccarelli, T., and Raghavan, M. (2023). Endo-lysosomal assembly variations among human leukocyte antigen class I (HLA class I) allotypes. eLife *12*, e79144. https://doi.org/10.7554/eLife.79144.
22. Blagoveshchenskaya, A.D., Thomas, L., Feliciangeli, S.F., Hung, C.H., and Thomas, G. (2002). HIV-1 Nef downregulates MHC-I by a PACS-1- and PI3K-regulated ARF6 endocytic pathway. Cell *111*, 853–866. https://doi.org/10.1016/s0092-8674(02)01162-5.
23. Kaksonen, M., and Roux, A. (2018). Mechanisms of clathrin-mediated endocytosis. Nat. Rev. Mol. Cell Biol. *19*, 313–326. https://doi.org/10.1038/nrm.2017.132.
24. Mayor, S., and Pagano, R.E. (2007). Pathways of clathrin-independent endocytosis. Nat. Rev. Mol. Cell Biol. *8*, 603–612. https://doi.org/10.1038/nrm2216.
25. Kovtun, O., Dickson, V.K., Kelly, B.T., Owen, D.J., and Briggs, J.A.G. (2020). Architecture of the AP2/clathrin coat on the membranes of clathrin-coated vesicles. Sci. Adv. *6*, eaba8381. https://doi.org/10.1126/sciadv.aba8381.
26. Collins, B.M., McCoy, A.J., Kent, H.M., Evans, P.R., and Owen, D.J. (2002). Molecular architecture and functional model of the endocytic AP2 complex. Cell *109*, 523–535. https://doi.org/10.1016/s0092-8674(02)00735-3.
27. Boulakirba, S., Macia, E., Partisani, M., Lacas-Gervais, S., Brau, F., Luton, F., and Franco, M. (2014). Arf6 exchange factor EFA6 and endophilin directly interact at the plasma membrane to control clathrin-mediated endocytosis. Proc. Natl. Acad. Sci. USA *111*, 9473–9478. https://doi.org/10.1073/pnas.1401186111.
28. Rennick, J.J., Johnston, A.P.R., and Parton, R.G. (2021). Key principles and methods for studying the endocytosis of biological and nanoparticle therapeutics. Nat. Nanotechnol. *16*, 266–276. https://doi.org/10.1038/s41565-021-00858-8.
29. Kumari, S., Mg, S., and Mayor, S. (2010). Endocytosis unplugged: multiple ways to enter the cell. Cell Res. *20*, 256–275. https://doi.org/10.1038/cr.2010.19.
30. Sannerud, R., Declerck, I., Peric, A., Raemaekers, T., Menendez, G., Zhou, L., Veerle, B., Coen, K., Munck, S., De Strooper, B., et al. (2011). ADP ribosylation factor 6 (ARF6) controls amyloid precursor protein (APP) processing by mediating the endosomal sorting of BACE1. Proc. Natl. Acad. Sci. USA *108*, E559–E568. https://doi.org/10.1073/pnas.1100745108.
31. Montealegre, S., Abramova, A., Manceau, V., de Kanter, A.F., and van Endert, P. (2019). The role of MHC class I recycling and Arf6 in

cross-presentation by murine dendritic cells. Life Sci. Alliance *2*, e201900464. https://doi.org/10.26508/lsa.201900464.

32. Li, L., Peng, X., Batliwala, M., and Bouvier, M. (2023). Crystal structures of MHC class I complexes reveal the elusive intermediate conformations explored during peptide editing. Nat. Commun. *14*, 5020. https://doi.org/10.1038/s41467-023-40736-6.
33. Frietze, K.K., Pappy, A.L., Melson, J.W., O'Driscoll, E.E., Tyler, C.M., Perlman, D.H., and Boulanger, L.M. (2016). Cryptic protein-protein interaction motifs in the cytoplasmic domain of MHCI proteins. BMC Immunol. *17*, 24. https://doi.org/10.1186/s12865-016-0154-z.
34. Xu, C., Gagnon, E., Call, M.E., Schnell, J.R., Schwieters, C.D., Carman, C.V., Chou, J.J., and Wucherpfennig, K.W. (2008). Regulation of T cell receptor activation by dynamic membrane binding of the CD3epsilon cytoplasmic tyrosine-based motif. Cell *135*, 702–713. https://doi.org/10.1016/j.cell.2008.09.044.
35. Yang, W., Pan, W., Chen, S., Trendel, N., Jiang, S., Xiao, F., Xue, M., Wu, W., Peng, Z., Li, X., et al. (2017). Dynamic regulation of CD28 conformation and signaling by charged lipids and ions. Nat. Struct. Mol. Biol. *24*, 1081–1092. https://doi.org/10.1038/nsmb.3489.
36. Wu, W., Zhou, Q., Masubuchi, T., Shi, X., Li, H., Xu, X., Huang, M., Meng, L., He, X., Zhu, H., et al. (2020). Multiple Signaling Roles of CD3epsilon and Its Application in CAR-T Cell Therapy. Cell *182*, 855–871.e823. https://doi.org/10.1016/j.cell.2020.07.018.
37. Wen, M., Cao, Y., Wu, B., Xiao, T., Cao, R., Wang, Q., Liu, X., Xue, H., Yu, Y., Lin, J., et al. (2021). PD-L1 degradation is regulated by electrostatic membrane association of its cytoplasmic domain. Nat. Commun. *12*, 5106. https://doi.org/10.1038/s41467-021-25416-7.
38. Parham, P., and Ohta, T. (1996). Population biology of antigen presentation by MHC class I molecules. Science *272*, 67–74. https://doi.org/10.1126/science.272.5258.67.
39. Jovanovic, O.A., Brown, F.D., and Donaldson, J.G. (2006). An effector domain mutant of Arf6 implicates phospholipase D in endosomal membrane recycling. Mol. Biol. Cell *17*, 327–335. https://doi.org/10.1091/mbc.e05-06-0523.
40. Wee, Y., Wang, J., Wilson, E.C., Rich, C.P., Rogers, A., Tong, Z., DeGroot, E., Gopal, Y.N.V., Davies, M.A., Ekiz, H.A., et al. (2024). Tumour-intrinsic endomembrane trafficking by ARF6 shapes an immunosuppressive microenvironment that drives melanomagenesis and response to checkpoint blockade therapy. Nat. Commun. *15*, 6613. https://doi.org/10.1038/s41467-024-50881-1.
41. Wonderlich, E.R., Leonard, J.A., Kulpa, D.A., Leopold, K.E., Norman, J.M., and Collins, K.L. (2011). ADP ribosylation factor 1 activity is required to recruit AP-1 to the major histocompatibility complex class I (MHC-I) cytoplasmic tail and disrupt MHC-I trafficking in HIV-1-infected primary T cells. J. Virol. *85*, 12216–12226. https://doi.org/10.1128/JVI.00056-11.
42. Radhakrishna, H., and Donaldson, J.G. (1997). ADP-ribosylation factor 6 regulates a novel plasma membrane recycling pathway. J. Cell Biol. *139*, 49–61. https://doi.org/10.1083/jcb.139.1.49.
43. D'Souza-Schorey, C., and Stahl, P.D. (1995). Myristoylation is required for the intracellular localization and endocytic function of ARF6. Exp. Cell Res. *221*, 153–159. https://doi.org/10.1006/excr.1995.1362.
44. Sanders, C.R., and Schwonek, J.P. (1992). Characterization of magnetically orientable bilayers in mixtures of dihexanoylphosphatidylcholine and dimyristoylphosphatidylcholine by solid-state NMR. Biochemistry *31*, 8898–8905. https://doi.org/10.1021/bi00152a029.
45. Delaglio, F., Grzesiek, S., Vuister, G.W., Zhu, G., Pfeifer, J., and Bax, A. (1995). NMRPipe: a multidimensional spectral processing system based on UNIX pipes. J. Biomol. NMR *6*, 277–293. https://doi.org/10.1007/BF00197809.
46. Bartels, C., Xia, T.H., Billeter, M., Güntert, P., and Wüthrich, K. (1995). The program XEASY for computer-supported NMR spectral analysis of biological macromolecules. J. Biomol. NMR *6*, 1–10. https://doi.org/10.1007/BF00417486.
47. Vranken, W.F., Boucher, W., Stevens, T.J., Fogh, R.H., Pajon, A., Llinas, M., Ulrich, E.L., Markley, J.L., Ionides, J., and Laue, E.D. (2005). The CCPN data model for NMR spectroscopy: development of a software pipeline. Proteins *59*, 687–696. https://doi.org/10.1002/prot.20449.
48. Kay, L.E., Ikura, M., Tschudin, R., and Bax, A. (2011). Three-dimensional triple-resonance NMR Spectroscopy of isotopically enriched proteins. 1990. J. Magn. Reson. *213*, 423–441. https://doi.org/10.1016/j.jmr.2011.09.004.
49. Salzmann, M., Wider, G., Pervushin, K., and Wüthrich, K. (1999). Improved sensitivity and coherence selection for [15N,1H]-TROSY elements in triple resonance experiments. J. Biomol. NMR *15*, 181–184. https://doi.org/10.1023/a:1008358030477.
50. Fu, Q., Piai, A., Chen, W., Xia, K., and Chou, J.J. (2019). Structure determination protocol for transmembrane domain oligomers. Nat. Protoc. *14*, 2483–2520. https://doi.org/10.1038/s41596-019-0188-9.

STAR★METHODS

KEY RESOURCES TABLE

REAGENT or RESOURCE	SOURCE	IDENTIFIER
Antibodies		
Mouse anti HA-Tag mAb	ABclonal	Cat# AE008; RRID: AB_2770404
GAPDH Mouse mAb	ABclonal	Cat# AC002; RRID: AB_2736879
Anti-HLA-A [Clone: EP1395Y]	Abcam	Cat# ab52922; RRID: AB_881225
Anti-HLA-ABC [Clone: w6/32]	Thermo Fisher Scientific	Cat# P105465; RRID: AB_468661
PE anti-human HLA-ABC [Clone: w6/32]	BioLegend	Cat# 311406; RRID: AB_314875
ARF6-Specific Polyclonal antibody	Proteintech	Cat# 20225-1-AP; RRID: AB_10646418
ARF6 Recombinant Rabbit monoclonal antibody [Clone: JF101-2]	HUABIO	Cat# ET1702-91; RRID: AB_3070350
ABflo® 488-conjugated Goat anti-Mouse IgG(H + L)	ABclonal	Cat# AS037; RRID: AB_2768319
ABflo® 488-conjugated Goat anti-Rabbit IgG(H + L)	ABclonal	Cat# AS053; RRID: AB_2768320
HRP-conjugated Goat anti-Mouse IgG(H + L)	ABclonal	Cat# AS003; RRID: AB_2769851
HRP-conjugated Goat anti-Rabbit IgG(H + L)	ABclonal	Cat# AS014; RRID: AB_2769854
Bacterial and virus strains		
BL21(DE3)	Tsingke	Cat# TSC-E01
E. coli DH5-alpha	Tsingke	Cat# TSC-C14
Chemicals, peptides, and recombinant proteins		
Isopropyl Alcohol	Macklin	Cat# I811925
Kanamycin monosulfate	Sangon Biotech	Cat# A600286
Ampicillin, Sodium Salt	Sangon Biotech	Cat# A610028
Methanol	Macklin	Cat# M813895
isopropyl β-D-thiogalatopyranoside (IPTG)	Sangon Biotech	Cat# A600168
Ammonium chloride (^{15}N, 99%)	Cambridge Isotope Laboratories	Cat# NLM-467-5
D-Glucose (U-$^{13}C_6$, 99%)	Cambridge Isotope Laboratories	Cat# CLM-1396-10
Imidazole	Sangon Biotech	Cat# I5513
Phenylmethanesulfonylfluoride (PMSF)	Sangon Biotech	Cat# A610425
DMPG Lipid	Avanti Polar Lipids	Cat# 840445
DMPC Lipid	Avanti Polar Lipids	Cat# 850345
DH_6PC Detergent	Avanti Polar Lipids	Cat# 850305
Gd-DOTA	Macrocyclics	Cat# M-147
Dithiothreitol(DTT)	Sangon Biotech	Cat# A620058
Penicillin-Streptomycin(100×)	Epizyme Biotech	Cat# CB010
Polybrene	Sigma-Aldrich	Cat# H9268
Cycloheximide(CHX)	AbMole	Cat# M4879
Octadecyl rhodamine B chloride (R18)	Invitrogen	Cat# O246
DMSO	Sangon Biotech	Cat# a600163
Deoxycholic acid, sodium salt	Sangon Biotech	Cat# A600150
CPP#: HLYVSPWGG	GenScript	N/A
CPP-WT#: HLYVSPWGGSSDSAQGSDVSLTACKV	GenScript	N/A
CPP-C363A#: HLYVSPWGGSSDSAQGSDVSLTAAKV	GenScript	N/A

(*Continued on next page*)

Continued

REAGENT or RESOURCE	SOURCE	IDENTIFIER
CPP-Irrelevant#: HLYVSPWGGSSDSAQGSDVSGGGGSS	GenScript	N/A
Critical commercial assays		
2× Universal SYBR Green Fast qPCR Mix	ABclonal	Cat# RK21203
ABScript *Neo* RT Master Mix for qPCR with gDNA Remover	ABclonal	Cat# RK20433
Seamless Cloning Kit	Beyotime	Cat# D7010
IP-ABE Palmitoylation Kit For WB	AIMSmass	Cat# AM10314
Deposited data		
HLA sequence database	IMGT	https://github.com/ANHIG/IMGTHLA
Experimental models: Cell lines		
Human: HEK-293T cells	ATCC	Cat# CRL-3216
Human: MCF7 cells	ATCC	Cat# HTB-22
Human: Raji cells	ATCC	Cat# CCL-86
Human: Jurkat cells	ATCC	Cat#TIB-152
Human: A549 cells	ATCC	Cat# CCL-185
Human: PANC-1 cells	ATCC	Cat# CRL-1469
Oligonucleotides		
GAPDH Fw: GGAGCGAGATCCCTCCAAAT	This paper	N/A
GAPDH Rv: GGCTGTTGTCATACTTCTCATGG	This paper	N/A
HLA-A Fw: AGATACACCTGTCACGTGCAGC	This paper	N/A
HLA-A Rv: GATCACAGCTCCAAGGAGAACC	This paper	N/A
Recombinant DNA		
P3EN-his-MBP-3C-HLA-A*1101_CTD(WT)	This paper	N/A
P3EN-his-MBP-3C-HLA-A*1101_CTD(L360A)	This paper	N/A
P3EN-his-MBP-3C-HLA-A*1101_CTD(T361A)	This paper	N/A
P3EN-his-MBP-3C-HLA-A*1101_CTD(C363A)	This paper	N/A
P3EN-his-MBP-3C-HLA-A*1101_CTD(K364A)	This paper	N/A
P3EN-his-MBP-3C-HLA-A*1101_CTD(V365A)	This paper	N/A
pcDNA3.1-10mer G12D-b2m-HA-HLA-A*1101(WT)-mTFP	This paper	N/A
pcDNA3.1-10mer G12D-b2m-HA-HLA-A*1101(Δ360-365)-mTFP	This paper	N/A
pcDNA3.1-10mer G12D-b2m-HA-HLA-A*1101(WT)-GFP	This paper	N/A
pcDNA3.1-10mer G12D-b2m-HA-HLA-A*1101(WT)-mCherry	This paper	N/A
pcDNA3.1-10mer G12D-b2m-HA-HLA-A*1101(Δ360-365)-GFP	This paper	N/A
pcDNA3.1-10mer G12D-b2m-HA-HLA-A*1101(Δ360-365)-mCherry	This paper	N/A
pcDNA3.1-10mer G12D-b2m-HA-HLA-A*1101(V358A)-GFP	This paper	N/A

(*Continued on next page*)

Continued

REAGENT or RESOURCE	SOURCE	IDENTIFIER
pcDNA3.1-10mer G12D-b2m-HA-HLA-A*1101(V358A)-mCherry	This paper	N/A
pcDNA3.1-10mer G12D-b2m-HA-HLA-A*1101(T361A)-GFP	This paper	N/A
pcDNA3.1-10mer G12D-b2m-HA-HLA-A*1101(T361A)-mCherry	This paper	N/A
pcDNA3.1-10mer G12D-b2m-HA-HLA-A*1101(C363A)-GFP	This paper	N/A
pcDNA3.1-10mer G12D-b2m-HA-HLA-A*1101(C363A)-mCherry	This paper	N/A
pcDNA3.1-10mer G12D-b2m-HA-HLA-A*1101(K364A)-GFP	This paper	N/A
pcDNA3.1-10mer G12D-b2m-HA-HLA-A*1101(K364A)-mCherry	This paper	N/A
pcDNA3.1-10mer G12D-b2m-HA-HLA-A*1101(V365A)-GFP	This paper	N/A
pcDNA3.1-10mer G12D-b2m-HA-HLA-A*1101(V365A)-mCherry	This paper	N/A
pcDNA3.1-10mer G12D-b2m-HA-HLA-A*1101(G310L/G314L)-GFP	This paper	N/A
pcDNA3.1-10mer G12D-b2m-HA-HLA-A*1101(G310L/G314L)-mCherry	This paper	N/A
pcDNA3.1-10mer G12D-b2m-HA-HLA-A*1101(G310L/G314L/Δ360-365)-GFP	This paper	N/A
pcDNA3.1-10mer G12D-b2m-HA-HLA-A*1101(G310L/G314L/Δ360-365)-mCherry	This paper	N/A
pcDNA3.1-10mer G12D-b2m-HA-HLA-A*1101(G310L/G314L/C363A)-GFP	This paper	N/A
pcDNA3.1-10mer G12D-b2m-HA-HLA-A*1101(G310L/G314L/C363A)-mCherry	This paper	N/A
PLEX-HA-HLA-A*1101(WT)	This paper	N/A
PLEX-HA-HLA-A*1101(Δ360-365)	This paper	N/A
PLEX-HA-HLA-A*1101(L360A)	This paper	N/A
PLEX-HA-HLA-A*1101(T361A)	This paper	N/A
PLEX-HA-HLA-A*1101(C363A)	This paper	N/A
PLEX-HA-HLA-A*1101(K364A)	This paper	N/A
PLEX-HA-HLA-A*1101(V365A)	This paper	N/A
PLEX-10mer G12D-b2m-HA-HLA-A*1101(WT)	This paper	N/A
PLEX-10mer G12D-b2m-HA-HLA-A*1101(Δ360-365)	This paper	N/A
PLEX-10mer G12D-b2m-HA-HLA-A*1101(L360A)	This paper	N/A
PLEX-10mer G12D-b2m-HA-HLA-A*1101(T361A)	This paper	N/A
PLEX-10mer G12D-b2m-HA-HLA-A*1101(C363A)	This paper	N/A
PLEX-10mer G12D-b2m-HA-HLA-A*1101(K364A)	This paper	N/A
PLEX-10mer G12D-b2m-HA-HLA-A*1101(V365A)	This paper	N/A
pcDNA3.1-ARF6	This paper	N/A
pcDNA3.1-ARF6-mTFP	This paper	N/A

(*Continued on next page*)

Continued

REAGENT or RESOURCE	SOURCE	IDENTIFIER
pcDNA3.1-eGFP	This paper	N/A
pcDNA3.1-mCherry	This paper	N/A
pcDNA3.1-eGFP-mCherry	This paper	N/A
Software and algorithms		
Sparky	Goddard, UCSF	www.cgl.ucsf.edu/home/sparky
NMRPipe	Delaglio, 1995	www.ibbr.umd.edu/nmrpipe
CCPNMR Analysis	Vranken, 2005	http://www.ccpn.ac.uk
Origin	OriginLab	www.originlab.com
PyMOL	Schrodinger, LLC	www.pymol.org
Adobe Illustrator 2020	Adobe	www.adobe.com/products/illustrator
Graphpad Prism 10	Graphpad	www.graphpad.com/scientific-software/prism
FlowJo	Becton, Dickinson & Company	www.flowjo.com
SnapGene	GSL Biotech	www.snapgene.com
ImageJ 1.8.0	Wayne Rasband	www.ImageJ.nih.gov/ij
Other		
DAPI	Beyotime	Cat# C1006
4% Paraformaldehyde Fix Solution	Ruian Biotech	Cat# R04-07A
Ni-NTA Beads	Smart-Lifesciences	Cat# SA004500
DpnI	NEB	Cat# R0176S
KOD One™ PCR Master Mix	TOYOBO	Cat# KMM101
Dialysis Membrane(MW:14000)	Biosharp	Cat# BS-QT-017-J
Superdex 75 Increase 10/300 GL Column	Cytiva	Cat# 29148721
Amicon Ultra Centrifugal Filter Units (10 kDa cut-off)	Millipore	Cat# UFC9010
Amicon Ultra Centrifugal Filter Units (3 kDa cut-off)	Millipore	Cat# UFC9003
Amicon Ultra Centrifugal Filter Units (3 kDa cut-off)	Millipore	Cat# UFC8003
HiPure Plasmid EF Mini Kit	Magen Biotech	Cat# P1112
HiPure Plasmid Maxi Kit	Magen Biotech	Cat# P1004
Anti-HA Nanobody Magarose Beads	Alpalife Biotech	Cat # KTSM1335
Polyethylenimine HCL Max, MW 40000	Polysciences	Cat # 24765
Protease inhibitor cocktail	ABclonal	Cat # RM02916
Bovine serum albumin, fraction V heat shock isolation	Sangon Biotech	Cat# A500023
Nonidet P-40	Sigma-Aldrich	Cat # 127087-87-0
Immobilon®-NC Transfer Membrane	Millipore	Cat# HATF00010
PageRuler Prestained Protein Ladder	Thermo Fisher scientific	Cat# 26616
Chemistar™ High-sig ECL Western Blotting Substrate	Tanon	Cat# 180-501

EXPERIMENTAL MODEL AND STUDY PARTICIPANT DETAILS

Cell lines and culture conditions

HEK293T, MCF-7, Raji, A549, Jurkat, and PANC-1 cells were obtained from the American Type Culture Collection (ATCC). HEK293T, MCF-7, A549, and PANC-1 cells were cultured in Dulbecco's modified Eagle's medium (DMEM), whereas Raji and Jurkat cells were maintained in RPMI 1640 medium. All media were supplemented with 10% fetal bovine serum and 1% penicillin-streptomycin. Cells were maintained at 37°C in a humidified incubator containing 5% CO_2.

METHOD DETAILS

Plasmid construction and mutagenesis

Full-length human HLA-A*11:01 constructs were generated in several configurations according to their experimental applications. Heavy-chain-only constructs encoded an N-terminally HA-tagged, full-length HLA-A*11:01 heavy chain without covalently linked peptide or β2-microglobulin (β2M), allowing noncovalent assembly with endogenous β2M and cellular peptides. The corresponding variants included WT, Δ360–365, L360A, T361A, C363A, K364A, and V365A.

Covalently linked single-chain peptide-MHC (pMHC) constructs contained the KRAS-G12D peptide, human β2M, an HA tag, and the full-length HLA-A*11:01 heavy chain connected by flexible peptide linkers. For flow cytometry based molecular proximity measurements, enhanced green fluorescent protein (eGFP) or mCherry was fused to the C terminus of the HLA-A cytoplasmic tail through a GSGGSG linker. The analyzed single-chain pMHC variants included WT, Δ360–365, V358A, T361A, C363A, K364A, V365A, the G310L/G314L transmembrane mutant (TM-mut), TM-mut + Δ360-365, and TM-mut + C363A. Unfused eGFP and mCherry were used as a negative FRET control, and a directly fused eGFP-mCherry construct was used as a positive control.

For acceptor-photobleaching FRET analysis of HLA-A cytoplasmic tail proximity to the plasma membrane, mTFP was fused to the C terminus of the WT or Δ360-365 single-chain pMHC construct. An ARF6-TFP construct was used to assess ARF6 proximity to the plasma membrane, and an untagged ARF6 expression construct was used for ARF6 overexpression experiments. Deletion and point mutant constructs were generated by site-directed mutagenesis using the corresponding WT plasmids as templates.

Protein expression and purification

The DNA sequence encoding the cytoplasmic tail of human HLA-A*11:01 (residues 333–365), designated HLA-A-CTD, was fused to an N-terminal 6×His maltose binding protein (MBP) tag followed by a PreScission protease (3C) cleavage site in the pET28a vector. The construct was transformed into Escherichia coli BL21 (DE3) cells and cultured in M9 minimal media at 37°C. Stable isotopes were supplemented to the media according to NMR experimental requirements. The culture was grown to an optical density at 600 nm (OD600) of 0.8–1.0, followed by induction with 0.2 mM isopropyl β-D-thiogalactopyranoside (IPTG) at 37°C for 4 h. Cells were harvested by centrifugation at 5000 rpm for 10 min at 4°C and stored at −80°C for downstream processing. The expressed fusion protein was extracted in Lysis Buffer (20 mM Tris-HCl, pH 8.0, 150 mM NaCl, 0.5 mM PMSF) and purified using nickel affinity resins (pre-equilibrated with Lysis Buffer containing 10 mM imidazole). The lysate was incubated with the resin for 1 h at 4°C on a rotator, followed by gravity flow to collect unbound fractions. The resin was washed extensively with Wash Buffer 1 (Lysis Buffer with 10 mM imidazole) and Wash Buffer 2 (Lysis Buffer with 20 mM imidazole) until no protein was detected in the flow-through. The bound protein was eluted with Elution Buffer (Lysis Buffer with 300 mM imidazole). The eluted protein was dialyzed overnight at 4°C against Lysis Buffer using a 14 kDa molecular weight cutoff membrane to remove high concentrations of imidazole. After dialysis, 3C protease was added at a ratio of 1:10 (w/w, enzyme: protein) and incubated at 4°C overnight to cleave the His tag. The protease digested mixture was reloaded onto the Ni-NTA resin to remove the 3C protease, uncleaved fusion protein, and any contaminating proteins bound to the resin. The flow-through and wash fractions (Wash Buffer 1) were collected, containing the cleaved HLA-A-CTD. The cleaved protein was concentrated using a centrifugal filter unit and subjected to size exclusion chromatography using a Superdex 75 Increase 10/300 GL column (29148721, Cytiva) equilibrated with FPLC Buffer (25 mM phosphate Buffer, pH 6.5, 100 mM NaCl). The purity and apparent molecular weight of HLA-A-CTD were assessed by SDS-PAGE.

Preparation of bicelle associated HLA-A-CTD for NMR measurements

To prepare bicelles for simulating membrane topology, 1,2-dimyristoyl-*sn*-glycero-3-phosphocholine (DMPC; 850345, Avanti Polar Lipids), 1,2-dimyristoyl-*sn*-glycero-3-phosphoglycerol (DMPG; 840445, Avanti Polar Lipids), and 1,2-dihexanoyl-*sn*-glycero-3-phosphocholine 6:0 PC (DH_6PC; 850305, Avanti Polar Lipids) were dissolved and mixed in chloroform at a molar ratio of 1:1.25. The mixture was dried slowly under a stream of nitrogen to form a thin film, followed by overnight lyophilization. The dried film was rehydrated in Phosphate Buffer A (25 mM phosphate Buffer, pH 6.5, 100 mM NaCl) to form bicelles. The HLA-A-CTD sample was mixed with the bicelle solution at a molar ratio of 2:1 and incubated overnight. If necessary, the q value of the bicelles was adjusted by adding additional DH_6PC or reducing its concentration through dialysis. The bicelle q value was maintained at approximately 0.8, as confirmed by NMR measurements, to mimic the topology of a lipid bilayer.

For most NMR experiments, the sample contained 500 μM HLA-A-CTD, 38 mM DMPC, 47 mM DH_6PC, 25 mM phosphate, 100 mM NaCl (pH 6.5), and 10% D_2O. At q = 0.8, the planar region of the bicelle has a radius of approximately 34 Å.[44]

Assignment of NMR resonances

All NMR experiments were conducted at 28°C using Agilent spectrometers operating at proton frequencies of 600 and 800 MHz and a Bruker spectrometer operating at 900 MHz, all equipped with cryogenic probes. The NMR data were processed using NMRPipe[45] and spectral analysis was performed with XEASY[46] and CcpNmr Analysis v.2.[47] For the sequence specific assignment of backbone chemical shifts of free HLA-A-CTD, TROSY enhanced triple resonance experiments were used.[48,49] These included HNCA, HN(CO)CA, HN(CA)CO, HNCO, HNCACB, and HN(CO)CACB. The experiments were recorded on a uniformly labeled (^{15}N, ^{13}C) HLA-A-CTD sample at 28°C and a proton frequency of 600 MHz.

Amino acid residues K335, S336, G341, and S343 were not assigned in the three-dimensional experiments due to weak signals. To address this issue, alanine point mutants were generated for each of these residues. NMR spectra were collected for the mutants under the same experimental conditions and compared with those of the wild-type protein. The mutation induced changes in chemical shifts successfully identified the corresponding assignments for these residues. Combining data from the triple resonance experiments with the mutant induced chemical shift changes, backbone chemical shifts were assigned for all observable residues.

Characterization of HLA-A-CTD membrane interaction using paramagnetic probe titration

The interaction between the 360–365 motif of HLA-A-CTD and the cell membrane was investigated using the paramagnetic probe titration (PPT) method.[50] Solvent PRE measurements were performed with 0.1 mM ^{15}N-labeled HLA-A-CTD (residues 333–365) in DMPC bicelles at a lipid-to-detergent ratio (q) of 0.8. The membrane inaccessible paramagnetic agent Gd-DOTA (M-147, Macrocyclics.) was titrated into the bicelle sample at concentrations of 0, 2, 4, 6, 8, and 10 mM. 2D ^{1}H-^{15}N TROSY-HSQC spectra were recorded at each titration point on an 800 MHz Agilent spectrometer (with recovery delay of 3 s). Residue-specific PRE was calculated as the ratio of peak intensities in the presence (I) and absence (I_0) of Gd-DOTA. Peak intensities were measured at local maxima and analyzed using quadratic interpolation to identify peak centers. The residue specific PRE amplitude (PRE_{amp}) was derived by fitting the I/I_0 ratio against the Gd-DOTA concentration using an exponential decay model, where τ represents the decay constant. For each of the residues, we used Origin (OriginLab, Northampton, MA) to fit the PRE titration curve to exponential decay to derive the residue-specific PRE amplitude (PRE_{amp}).

$$\frac{I}{I_0} = 1 - PRE_{amp}\left(1 - e^{-\frac{[Gd-DOTA]}{\tau}}\right) \quad \text{(Equation 1)}$$

Assignment of NOE restraints

The NOE restraints were obtained using selectively labeled HLA-A cytoplasmic tail (CTD) samples reconstituted in bicelle systems. Mixtures of uniformly ^{15}N/^{2}H-labeled CTD with ^{13}C-labeled CTD were prepared at a 1:1 molar ratio. Bicelles for interchain NOE detection were prepared using DMPC and DHPC at a *q* value of 0.8. The spectrum was acquired at 900 MHz. Dimer formation in bicelles was evaluated using 2D NOE difference ^{1}H-^{15}N TROSY-HSQC experiments, recorded as interleaved spectra with and without NOE mixing (τ_NOE = 200 ms), enabling verification of NOE dependent signal differences under membrane mimetic conditions.

Quantitative measurement of fluorescence resonance energy transfer (FRET)

To study membrane interactions, mTFP was fused to the C terminus of covalently linked WT or Δ360-365 single-chain pMHC constructs comprising the KRAS-G12D peptide, human β2M, an HA tag, and the full-length HLA-A*11:01 heavy chain. These plasmids were packaged into lentiviral particles and transduced into 293T cells to generate stable cell lines. After culturing to the appropriate density, 5×10^5 cells were counted, resuspended in 1 mL DMEM, and seeded onto the center of a 25-mm glass-bottom culture dish. The plates were incubated overnight at 37°C to allow cell adhesion. On the following day, excess media were removed by washing with 1 mL ice-cold PBS. Cells were then stained with 2 μM octadecyl rhodamine B (R18, O246, Invitrogen) for 5 min at room temperature. Following staining, residual dye was removed by two PBS washes, and fresh DMEM (1 mL) was added to the dish. FRET efficiencies between mTFP (donor) and R18 (acceptor) were quantified using a fluorescence microscope (Zeiss LSM 710×, 100× oil-immersion objective). Donor fluorescence was monitored by exciting mTFP at 458 nm and detecting at 470–550 nm, while acceptor fluorescence was excited at 561 nm and detected at 570–650 nm. R18 was fully photobleached by illuminating cells with a 561-nm laser at 100% efficiency for 60 s. TFP fluorescence intensities were recorded three times both before and after R18 photobleaching. FRET efficiencies were calculated using the following equation:

$$FRET_{eff} = \frac{FL_{AP} - FL_{BP}}{FL_{AP}} \quad \text{(Equation 2)}$$

where FL_{AP} and FL_{BP} represent mTFP fluorescence after and before R18 photobleaching, respectively.

For analysis of ARF6-plasma membrane proximity, ARF6-TFP was expressed in 293T cells carrying WT or Δ360-365 single-chain pMHC constructs. ARF6-TFP served as the FRET donor, and membrane localized R18 served as the acceptor. Cells were stained with 2 μM R18 and analyzed by acceptor-photobleaching FRET using the same imaging, photobleaching, and calculation procedures described above.

Non-reducing SDS-PAGE analysis of purified HLA-A*11:01 CTD

Purified HLA-A*11:01 CTD samples were mixed with 5× SDS loading buffer lacking reducing agents, such as β-mercaptoethanol or dithiothreitol, at a 4:1 volume ratio and incubated for 20 min at room temperature before electrophoresis. For samples incubated with DMPC bicelles, the final protein concentration was 50 μM. DMPC bicelles were added at protein-to-bicelle molar ratios ranging from 1:0 to 1:0.75, and the samples were incubated for 1 h at room temperature with gentle rotation. After incubation, 5× non-reducing SDS loading buffer was added as described above. Equal amounts of each protein sample and a protein molecular weight marker

(26616, Thermo Fisher Scientific) were loaded onto a precast gradient polyacrylamide gel. Electrophoresis was performed at 150 V in 1× MES running buffer containing 50 mM MES, 50 mM Tris base, 0.1% SDS, and 1 mM EDTA, pH 7.3, until the bromophenol blue dye front reached the bottom of the gel.

After electrophoresis, the gel was carefully removed and washed several times with deionized water. The gel was fixed for 15 min at room temperature, stained with Coomassie Brilliant Blue for 30 min at room temperature with gentle agitation, and subsequently destained until the protein bands were clearly visible against a transparent background. Gel images were acquired using a gel documentation system.

Flow cytometry analysis

Endocytosis rate analysis

For the main figure experiments, pooled stable MCF7 populations expressing heavy-chain-only HLA-A*11:01 WT, Δ360-365, or the indicated point-mutant constructs were used. For the corresponding supplemental experiments, monoclonal 293T cell lines expressing WT or mutant single-chain pMHC constructs were analyzed. Cells were harvested by centrifugation at 500 × g for 3 min and washed two to three times with PBS. The cells were then resuspended in 500 μL PBS and incubated with mouse anti-HA antibody (AE008, ABclonal; 1:1,000 dilution) for 1 h at 4°C to label surface exposed HLA-A while minimizing membrane trafficking.

After incubation, unbound primary antibody was removed by washing the cells two to three times with PBS followed by centrifugation at 500 × g for 3 min. The cell suspension was then divided into aliquots for the indicated time points. For the 0-min sample, one aliquot was immediately resuspended in 100 μL PBS and incubated with FITC-conjugated anti-mouse secondary antibody (AS037, ABclonal; 1:100 dilution) for 15 min at 4°C in the dark. The remaining aliquots were resuspended in complete DMEM and incubated at 37°C to allow internalization. At the indicated time points, cells were collected, washed two to three times with ice-cold PBS, and stained with the same FITC-conjugated secondary antibody for 15 min at 4°C in the dark. After staining, unbound secondary antibody was removed by washing as described above.

Fluorescence signals were quantified by flow cytometry and analyzed using FlowJo software. Surface-accessible fluorescence at each time point was normalized to the corresponding 0-min value for each construct, thereby reporting the fraction of the initially labeled HLA-A pool that remained accessible at the cell surface.

*Flow cytometry-based FRET analysis of relative proximity between single-chain HLA-A*11:01 pMHC constructs*

Covalently linked single-chain pMHC constructs comprising the G12D peptide, human β2M, and full-length HLA-A*11:01 heavy chain were used for flow cytometry-based FRET measurements. eGFP or mCherry was fused to the C terminus of the HLA-A cytoplasmic tail through a GSGGSG linker. The analyzed variants included WT, Δ360–365, C363A, K364A, V358A, T361A, V365A, the G310L/G314L transmembrane mutant (TM-mut), TM-mut + Δ360-365, and TM-mut + C363A. Residue numbering refers to the HLA-A*11:01 heavy chain. When the cell density of 293T cells reached 70–80% confluency, cells were transfected with 1.5 μg of each plasmid per well using standard transfection protocols. After 24 h, cells were collected by centrifugation at 500× g for 3 min, washed 2–3 times with 1× PBS, and resuspended in an appropriate volume of PBS. The cell suspension was passed through a cell strainer to remove aggregates and subjected to flow cytometry analysis. Flow cytometry was performed on a BD analyzer equipped with blue (488 nm) and green (561 nm) lasers. eGFP fluorescence was detected using a 530/30 nm filter off the blue laser, and mCherry fluorescence was measured using a 610/20 nm filter off the green laser. FRET emission was collected through the 610/20 nm detector off the blue laser. Data were analyzed using FlowJo v10 (BD Biosciences) to quantify eGFP-positive, mCherry-positive, eGFP/mCherry double-positive, and FRET-positive populations.

Surface HLA-I analysis after peptide treatment

The peptides used in this study, including CPP, CPP-WT, CPP-C363A, and CPP-Irrelevant, were synthesized by GenScript Biotech Corporation (Shanghai, China) and purified by high-performance liquid chromatography to a purity greater than 95%. Lyophilized peptides were dissolved in dimethyl sulfoxide (DMSO) to prepare 10 mM stock solutions, aliquoted, and stored at −20°C. Before use, the stock solutions were diluted in culture medium to the indicated working concentrations.

Raji, A549, and PANC-1 cells were seeded into 12-well plates and treated with the indicated peptides for 12 h. A549 and PANC-1 cells were treated when they reached approximately 60%–70% confluence. The peptide concentrations used for Raji, A549, and PANC-1 cells were 1 μM, 10 μM, and 5 μM, respectively. After treatment, cells were collected and washed two to three times with PBS. Cells were resuspended in 100 μL PBS and incubated with PE-conjugated anti-human HLA-ABC antibody (311406, BioLegend; 1:200 dilution) for 20 min at 4°C. Cells were then centrifuged at 500 × g for 3 min at 4°C and washed two to three times with PBS. Surface HLA-I fluorescence was measured by flow cytometry, and the data were analyzed using FlowJo software.

The following flow cytometry antibody labeling and detection of biomarker abundance on the cell surface, including the required quantities and incubation times, were identical to the steps described above.

Western blot

Acyl-biotin exchange (ABE) assay for MHC-I palmitoylation

293T cells stably expressing HA-tagged MHC-I WT or C363A were pelleted (500 × g, 3 min), washed 2–3× with ice-cold PBS, and lysed in EBC Buffer (50 mM Tris-HCl pH 8.0, 150 mM NaCl, 0.5% NP-40) with protease inhibitors (30 min, on ice). Lysates were cleared (12,000 rpm, 15 min, 4°C), and supernatants incubated O/N at 4°C with anti-HA magnetic beads (KTSM1335, AlphaLifeBio). Palmitoylation analysis used the IP-ABE Kit (AM10314, AIMSmass) per manufacturer. Beads were washed with

500 μL PBS, then incubated with 300 μL Buffer 3 + 100 μL Buffer 2 (30 min, RT). After separation, 485 μL Buffer 3 + 10 μL Buffer 4 + 5 μL 0.1 M PMSF were added (3 h, RT, dark). Beads were washed and resuspended in 485 μL Buffer 3. For WT, parallel +HA and −HA tubes were set. Buffer 5 (200 μL) was added to WT (+HA) and C363A; Buffer 6 (200 μL) to WT (−HA) (1 h, RT). After separation, 480 μL Buffer 3 + 20 μL Buffer 7 were added (1 h, RT), beads washed 2× with 500 μL Buffer 3, then eluted with 60 μL 1× SDS loading buffer (99°C, 10 min). Equal volumes were analyzed by SDS-PAGE/Western blot.

Non-reducing immunoblots analysis of cellular HLA-A species

Jurkat and Raji cells were harvested and washed twice with PBS. Cells were lysed on ice for 30 min in RIPA lysis buffer containing protease inhibitors (RM02916, ABclonal). The RIPA buffer consisted of 50 mM Tris-HCl, pH 8.0, 150 mM NaCl, 0.1% SDS, 0.5% sodium deoxycholate, and 1% Triton X-100. Cell lysates were centrifuged at 12,000 rpm for 15 min at 4°C, and the supernatants were collected. Samples were mixed with 5× SDS loading buffer lacking reducing agents, such as β-mercaptoethanol or dithiothreitol (DTT). In parallel, reducing control samples were prepared by adding excess DTT. Proteins were separated by SDS-PAGE and transferred to nitrocellulose membranes (HATF00010, Millipore). Membranes were blocked with 5% non-fat milk in TBS-T for 1 h at room temperature and washed three times with TBS-T. The membranes were incubated overnight at 4°C with rabbit anti-HLA-I antibody (ab52922, Abcam) and mouse anti-GAPDH antibody (AC002, ABclonal). After three washes with TBS-T, the membranes were incubated separately with the corresponding HRP-conjugated secondary antibodies, anti-mouse HRP (AS003, ABclonal) or anti-rabbit HRP (AS014, ABclonal), for 1 h at room temperature. Following three additional washes with TBS-T, chemiluminescent signals were developed using ECL substrate (180–501, Tanon) and acquired using a Tanon 5200CE imaging system.

Cycloheximide-chase analysis of HLA-A protein turnover

Bulk stable 293T populations expressing heavy-chain-only HLA-A*11:01 WT or Δ360-365 constructs, as well as monoclonal 293T lines expressing the corresponding single-chain pMHC constructs, were cultured to 80%–90% confluence and treated with cycloheximide (M4879, AbMole) at a final concentration of 100 μg/mL. For the peptide-treatment experiments, 293T cells stably expressing heavy-chain-only WT HLA-A*11:01 were treated with DMSO or 10 μM CPP-WT, CPP-C363A, CPP alone, or CPP-Irrelevant during the cycloheximide chase. Cells were harvested at the indicated time points by centrifugation. After resuspension in RIPA lysis buffer (50 mM Tris-HCl, pH 8.0, 150 mM NaCl, 0.1% SDS, 0.5% sodium deoxycholate, and 1% Triton X-100) containing protease inhibitors (RM02916, ABclonal), cells were incubated on ice for 30 min. Cell lysates were centrifuged at 12,000 rpm for 15 min at 4°C, and the supernatants were collected. Protein samples were mixed with 5× loading buffer and denatured at 99°C for 10 min. Proteins were separated by SDS-PAGE and transferred to nitrocellulose membranes (HATF00010, Millipore). Membranes were blocked with 5% non-fat milk (A600669, Sangon Biotech) in TBS-T for 1 h, followed by three washes with TBS-T. Membranes were incubated overnight at 4°C with mouse anti-HA antibody (AE008, ABclonal). The following day, membranes were washed three times with TBS-T and incubated with HRP-conjugated anti-mouse secondary antibody (AS003, ABclonal) for 1 h at room temperature. Chemiluminescent signals were detected using a Tanon 5200CE imaging system with ECL substrate (180–501, Tanon) and quantified using ImageJ.

IP-MS for MHC-I

HA-MHC-I WT 293T stable cells were harvested and resuspended in EBC buffer (50 mM Tris-HCl, pH 8.0, 150 mM NaCl, 0.5% NP-40), supplemented with appropriate protease inhibitors, and lysed on ice for 30 min. The lysate was centrifuged at 12,000 rpm for 15 min at 4°C, and the supernatant was collected. The supernatant was incubated with pre-equilibrated anti-HA magnetic beads (KTSM1335, AlphaLifeBio) at 4°C overnight. The following day, magnetic beads were captured using a magnetic rack, and the supernatant was discarded. The beads were washed five times with NETN Buffer (20 mM Tris-HCl, pH 8.0, 100 mM NaCl, 1 mM EDTA, 0.5% NP-40). To elute the bound proteins, 60 μL of 1× loading buffer was added to the beads, and the samples were heated in a metal bath at 99°C to partially dry to an appropriate volume. Protein samples were separated by SDS-PAGE, and the gel was stained with Coomassie Brilliant Blue. The corresponding band region was excised and transferred to a 1.5 mL EP tube for subsequent mass spectrometry analysis.

Co-IP for MHC-I and ARF6

For the main figure experiments, HA-tagged heavy-chain-only WT or Δ360-365 HLA-A*11:01 constructs were expressed in A549 and PANC-1 cells. For the corresponding supplemental experiments, HA-tagged WT or Δ360-365 single-chain pMHC constructs were expressed in 293T and A549 cells. Equal numbers of cells were lysed in EBC buffer (50 mM Tris-HCl, pH 8.0, 150 mM NaCl, and 0.5% NP-40) containing protease inhibitors for 30 min on ice. Lysates were clarified by centrifugation at 12,000 rpm for 15 min at 4°C. The supernatants were incubated overnight at 4°C with anti-HA magnetic beads (KTSM1335, AlphaLifeBio). The beads were washed five times with NETN buffer and eluted by adding 60 μL of 1× loading buffer followed by heating at 99°C for 10 min. Eluates were resolved by SDS-PAGE and transferred to nitrocellulose membranes (HATF00010, Millipore). Membranes were blocked with 5% non-fat milk in TBS-T for 1 h at room temperature, washed three times, and incubated overnight at 4°C with mouse anti-HA antibody (AE008, ABclonal) and rabbit anti-ARF6 antibody (ET1702-91, Huabio, 1:2,000 dilution). Membranes were then washed and incubated with HRP-conjugated anti-mouse or anti-rabbit secondary antibodies (AS003 and AS014, respectively; ABclonal) for 1 h at room temperature. After three washes, chemiluminescent signals were developed using ECL substrate (180–501, Tanon), detected using a Tanon 5200CE imaging system, and quantified with ImageJ.

qRT-PCR analysis

Pooled stable MCF7 populations expressing heavy-chain-only HLA-A*11:01 WT or Δ360-365 constructs were used for the main-figure analysis. Monoclonal 293T cell lines expressing the corresponding WT or Δ360-365 single-chain pMHC constructs were

analyzed in parallel for the supplemental experiment. Five million cells per sample were harvested, and total RNA was extracted using a commercial RNA purification kit (RK30120, ABclonal) according to the manufacturer's instructions, including genomic DNA removal. RNA concentration was measured, and 1 μg of total RNA was used for cDNA synthesis using a reverse-transcription kit (RK20433, ABclonal).

Quantitative PCR reactions were performed in a total volume of 20 μL containing 1 μL cDNA, 10 μL SYBR Green Master Mix (RK21203, ABclonal), 0.4 μL each of forward and reverse primers from 10 μM stocks, and 8.2 μL ddH_2O. Reactions were run on a QuantStudio 7 Pro Real-Time PCR System according to the manufacturer's instructions. HLA-A transcript abundance was normalized to GAPDH, and the WT group was set to 1. The primer sequences were as follows:

- GAPDH FW: GGAGCGAGATCCCTCCAAAT
- GAPDH RV: GGCTGTTGTCATACTTCTCATGG
- HLA-A FW: AGATACACCTGTCACGTGCAGC
- HLA-A RV: GATCACAGCTCCAAGGAGAACC

QUANTIFICATION AND STATISTICAL ANALYSIS

All statistical analyses were performed using GraphPad Prism software (GraphPad Software). Experimental data are presented as mean ± standard deviation (SD), and error bars in the figures represent SD. Sample sizes (n) and the numbers of independent experiments are specified in the corresponding figure legends. Comparisons between two groups were performed using two-tailed Student's *t* tests. Comparisons among multiple groups with a single reference group were performed using one-way analysis of variance (one-way ANOVA) followed by Dunnett's multiple-comparisons test. Time-course experiments with two independent variables, including cycloheximide-chase and internalization assays, were analyzed using two-way ANOVA followed by Dunnett's multiple-comparisons test. A p value < 0.05 was considered statistically significant. Statistical significance is indicated as follows: ns, not significant; $^{*}p < 0.05$; $^{**}p < 0.01$; and $^{***}p < 0.001$.